Evolving Earth 3 (2025) 100063

Contents lists available at ScienceDirect

Evolving Earth

journal homepage: www.sciencedirect.com/journal/evolving-earth

Contact metamorphism of coals in the Southern Piceance Basin, USA: Volatile matter generation, pyrolytic carbon accumulation, and $\delta^{13}C$ trends

Susan M. Rimmer [a,*], Lois E. Yoksoulian [b], Darren R. Gröcke [c]

[a] School of Earth Systems and Sustainability, Southern Illinois University Carbondale, Carbondale, IL, 62901, United States
[b] University of Illinois News Bureau, University of Illinois at Urbana-Champaign, Champaign, IL, 61822, United States
[c] Department of Earth Sciences, Durham University, Science Labs, Durham, DH1 3LE, United Kingdom

ARTICLE INFO

Keywords:
Sill intrusion
Pyrolytic carbon
Carbon isotopes
Coked coal
Methane

ABSTRACT

Four transects of coal were studied to determine petrographic, geochemical, and $\delta^{13}C$ changes due to contact with thin sills. Approaching the sills, vitrinite and coke reflectance increases from ~0.75% to ~7%, while volatile matter (VM) and H/C decrease. Despite extensive VM loss, the coals do not follow normal burial maturation pathways. Alteration above the sills exceeds that below, and the width of the contact aureole is large compared to that of the sills. This may suggest prolonged magma transport within the sills. Additionally, multiple fractures contain coke, pyrolytic carbon, and minerals, which suggests migration of fluidized coal, VM, and hot fluids. Incipient mosaic and anisotropic coke structures (fine-grained circular mosaic, with minor medium-grained circular mosaic) are observed within the aureole, consistent with intrusion of a high volatile bituminous coal. Devolatilization vacuoles, more abundant in altered collodetrinite than collotelinite, increase in number and size approaching the sills. Pyrolytic carbon occurs as fracture fills, spherulites, and botryoidal aggregates; spherulitic forms are more abundant at higher maturation levels. $\delta^{13}C$ of the altered coal/coke varies only minimally from that of the unaltered coal and overall trends are ambiguous. Factors affecting $\delta^{13}C$ may include maceral composition, rank at the time of intrusion, extent of alteration, size of the carbon reservoir, redeposition of pyrolytic carbon, and openness of the system. It is possible that the rapid heating and high temperatures associated with contact metamorphism limit carbon isotopic fractionation. In turn, this may imply that the intrusion of coal results in minimal liberation of isotopically light CH_4.

1. Introduction

During Earth's history, there have been periods of global warming associated with marine extinction events such as the Paleocene-Eocene Thermal Maximum (PETM) (~55 Ma), the Toarcian-Oceanic Anoxic Event (T-OAE) (~183 Ma), and the end-Permian event (252 Ma) that are represented by $\delta^{13}C$ excursions in the sedimentary record (see Hesselbo et al., 2000; McInerney and Wing, 2011; Caruthers et al., 2013; Burgess et al., 2017; Trabucho-Alexandre et al., 2022). It has been suggested that these events were associated with the release of greenhouse gases (CH_4 and/or CO_2) by destabilization of CH_4 hydrates from continental shelves (Dickens et al., 1995; Krull et al., 2000, 2004; Beerling et al., 2002), desiccation of organic matter (OM) along a large epicontinental seaway (Higgins and Schrag, 2006), the intrusion of igneous rocks into organic-rich shales and coals (Svensen et al., 2004; McElwain et al., 2005; Retallack and Jahren, 2008; Aarnes et al., 2010; Grasby et al., 2011; Rampino et al., 2017), or a combination of effects (Pagani et al., 2006). The volume and rate at which these gases would have been released by these mechanisms, and their impact on the isotopic signature of the atmosphere has been debated (Gröcke et al., 2009).

The intrusion of magma into organic-rich shale and coal would presumably result in the release of thermogenic gases including CO_2 and CH_4 that would contribute to global climate change (Hesselbo et al., 2000; Svensen et al., 2004, 2007; McElwain et al., 2005). Such thermal alteration of OM would be expected to leave behind a residual carbon that is enriched in ^{13}C relative to the unaltered coal or other OM, as ^{12}C–^{12}C bonds are easier to break and therefore the gases generated would be ^{12}C-enriched (Hoefs and Frey, 1976; Conkright and Sackett, 1992; Schimmelmann et al., 2009). For example, it has been shown experimentally that CH_4 derived from coal is 25‰ lighter than the coal

This article is part of a special issue entitled: coal published in Evolving Earth.

* Corresponding author.
E-mail address: srimmer@siu.edu (S.M. Rimmer).

https://doi.org/10.1016/j.eve.2025.100063
Received 23 November 2024; Received in revised form 16 January 2025; Accepted 12 February 2025
Available online 14 February 2025

itself (Hoefs and Frey, 1976; Sackett, 1978). Studies have shown that highly metamorphosed OM can have $\delta^{13}C_{org}$ values that are significantly heavier (14‰) compared to unmetamorphosed OM (Hoefs and Frey, 1976). However, data from the literature show mixed results. Whereas some studies have suggested small changes towards heavier $\delta^{13}C_{org}$ in intruded OM (e.g., Saxby and Stephenson, 1987), others have shown minimal or ambiguous changes (Schimmelmann et al., 2009; Yoksoulian, 2010; Yoksoulian et al., 2016; Rahman et al., 2017, 2018). Still other authors have reported more negative $\delta^{13}C_{org}$ values in coals adjacent to intrusions (Meyers and Simoneit, 1999; Cooper et al., 2007). One complication could be the formation of neoformed components such as pyrolytic carbon, deposited from trapped volatile matter (VM), that could lead to more negative $\delta^{13}C_{org}$ values in the residual coal or coke (Meyers and Simoniet, 1999; Cooper et al., 2007; Sanders et al., 2023). In addition, the very large size of the carbon reservoir in the residual coal may result in only minor changes in $\delta^{13}C_{org}$ values (Whiticar, 1996) and the expected changes may only be seen in relatively low-carbon samples (Sanders and Rimmer, 2023).

In the current study, organic petrography, bulk geochemistry, and stable isotope geochemistry are presented for samples collected from a coal face at an underground mine and from three nearby cores on the mine property (Bowie Mine, Somerset Coalfield, Piceance Basin, Colorado, USA). At this location, the coal seams had been intruded (and possibly partially replaced) by sills. The objectives of the study were to: 1) evaluate petrographic changes in the coal due to heating by the sills, including evidence of coking and formation of pyrolytic carbon; 2) evaluate geochemical changes in the coal approaching the sill; and 3) determine whether $\delta^{13}C_{org}$ values of the residual coal were significantly affected by the intrusion.

1.1. Geologic setting

The Piceance Basin is bounded by the Uinta Mountains and Axial Basin anticline in the north, the Uncompahgre Uplift in the west, the Gunnison Uplift and West Elk Mountains in the south, and the White River Uplift and Elk Mountains in the east (Sanborn, 1977; Cole and Cumella, 2003). The Cretaceous coal-bearing strata of the Mesaverde Group were deposited as marshes and mires formed along coastal-plain environments during isostatic sea-level changes within the Western Interior Seaway related to the Sevier orogeny (Cole and Cumella, 2003; Carroll et al., 2004). During the Cretaceous, this part of Colorado was ~42° N and experienced a humid, subtropical climate (Roberts and Kirschbaum, 1995; Hettinger et al., 2000). The peats that resulted in the coals at the Bowie Mine accumulated during the latest Campanian and early Maastrichtian (~70 Ma) (Franczyk et al., 1992; Robeck, 2005). Within the southern part of the basin (the locale for this study), peat accumulation resulted in commercially viable coals in six distinct coalfields, namely the Book Cliffs, Grand Mesa, Somerset, Crested Butte, Carbondale, and Grand Hogback that crop out along the edge of the Piceance Basin (Fig. 1) (Hettinger et al., 2000; Carroll et al., 2004).

In the Piceance Basin, Late Cretaceous to Early Tertiary Laramide deformation folded and faulted the region, forming a topographic depression, followed by Cenozoic deposition. The basin is strongly asymmetric with its fold axis along the eastern edge of its surface expression (Cole and Cumella, 2003). Cenozoic igneous activity within the southern portion of the Piceance Basin (Knopf, 1926; Obradovich et al., 1969; Cole and Cumella, 2003; Carroll et al., 2004) produced the Elk Mountain, Ruby Range, and West Elk Mountain igneous complexes and numerous mafic sills that contact the near-horizontal, coal-bearing strata in this area (Obradovich et al., 1969; Carroll et al., 2004). Coal rank is generally medium to high volatile bituminous, although it increases to anthracite in areas affected by igneous bodies (Carroll et al., 2004). Field relationships and petrographic observations indicate that the igneous activity occurred in four separate events (Obradovich et al., 1969). The earliest stage involved the emplacement of felsic sills (Knopf, 1926) along the west margin of the Sawatch Range (Obradovich et al., 1969). The second phase was marked by the emplacement (~34–79 Ma) of granodioritic stocks, laccoliths, sills, and dikes of the Elk Mountains, Ruby Range, and West Elk Mountains (Obradovich et al., 1969). In stage three, porphyritic gabbro and ultramafic dikes and sills crosscut these structures and later sedimentary units (Mesaverde Formation), most notably in the West Elk Mountains, where the Bowie Mine is located (Obradovich et al., 1969; Carroll et al., 2004). The final stage involved the emplacement of a highly localized and unique soda granite exposed near the town of Marble, Colorado (Obradovich et al., 1969).

Basin modelling has suggested that the coals reached near modern-

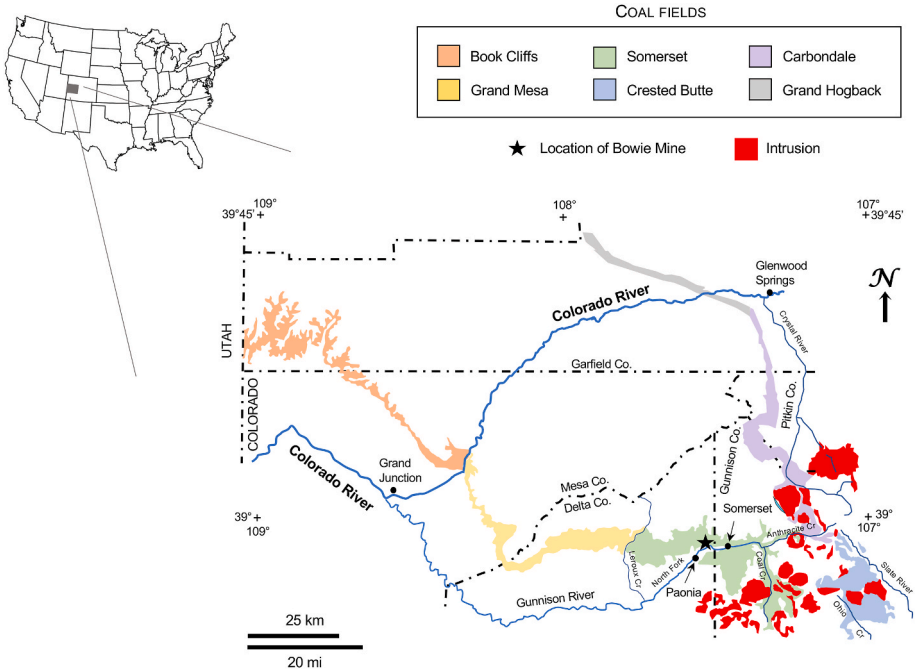

Fig. 1. Map showing Bowie Mine location in context of coalfields of the southern Piceance Basin (base map modified from Hettinger et al., 2000). Note: Laccoliths shown for the area around the Somerset, Crested Butte, and southern part of the Carbondale coalfields.

day rank levels by the end of the Eocene (~34 Ma) (Johnson and Nuccio, 1986; Robeck, 2005), with rank increase due to burial depths rather than igneous activity (Johnson and Nuccio, 1986). Subsequently, localized increases in rank and alteration accompanied emplacement of igneous bodies during the Miocene: an intermediate stock, the Iron Point stock, was emplaced just to the northeast (~1.5–2 km away) of the Bowie Mine at 14.7 ± 1.1 Ma, basaltic lava flows (up to 225m) were deposited on Grand Mesa to the west around 11 Ma, basaltic sills intruded the coals at the mine at 9.59 ± 0.12 Ma (Late Miocene), and a series of basaltic dikes on Grand Mesa formed around 6.75 ± 0.15 Ma (Robeck, 2005). Robeck (2005) suggested that three sills migrated several kilometers along coal seams in the Bowie Mine area, melting and devolatilizing the seams over a wide area; a comparison of seam thickness for intruded vs. un-intruded areas, suggests this resulted in a significant loss in coal volume, averaging 25% but perhaps even greater volumes (as much as 80%) adjacent to the thicker seams.

2. Sampling and methods

2.1. Sampling

Four sample transects were collected from the DU and BU seams of the Upper Cretaceous Coal-bearing Member of the Mesaverde Formation within the Somerset Coalfield in west-central Colorado (Fig. 2). These are high volatile bituminous coals that were intruded by Cenozoic igneous sills. This coalfield is the southernmost of the six distinct Late Cretaceous-age Mesaverde fields (Fig. 1) (Hettinger et al., 2000). Samples were collected at the Bowie Mine, an active (at the time, 2008) underground mine operated by Bowie Resources, LLC, near Paonia, Delta County, Colorado (Fig. 1). One suite of samples was collected from a previously mined face of the DU seam. Within this mine, a sill of varying thickness had intruded along the top of the coal, and multiple exposures of coke "fingers" were evident (Fig. 3). At this location, a total of seven samples (T1–T7) were collected from the seam with the transect extending from the base of a roof-level sill (0.5m thick) down to the mine floor (~1.7m) (Table 1). The extreme hardness of the highly metamorphosed coal did not permit channel sampling, and thus “grab” samples were collected.

Three additional transects were collected from areas where the BU seam had been intruded (directly below the active mine) using exploration cores: DD-NM3-53-56 (core 1, samples 1.1–1.18), DD-NM6X90-40 (core 2, samples 2.2–2.14), and DD-NM6X76-44 (core 4, samples 4.2–4.22) (Table 1). Core 4 was located ~900m from core 1, and core 2 was ~650m from core 4 (based on Fig. 2.7 in Yoksoulian, 2010). Core samples were collected using a similar technique to that used for the mine face samples; however, due to interbedding with other sedimentary rocks (not sampled) within the cores, intervals were less evenly spaced than at the mine face. Within the cores, elevations and thicknesses of the sill differ slightly at each location, due in part to orientation of the sill, the local dip of the bedding, and faulting within the mine (Carroll et al., 2004). Mine personnel indicated that there are most likely both single and multiple sills that interfinger with varying stratigraphic units. Two of the sampled series (the mine face and core 1 samples) were adjacent to sills that are slightly thicker, 0.5m and 0.62m, respectively. The other two series (cores 2 and 4) were adjacent to much thinner sills, 0.08m and 0.05m, respectively. However, the sills were reported to be much thicker beyond the active mine; for example, the sill intruding the BU seam increased in thickness towards the NW and W, exceeding 7–9m in places (Robeck, 2005).

2.2. Petrographic and geochemical analyses

All samples were thoroughly washed to remove excess dirt and rock dust before further preparation. After ambient drying, samples were crushed to minus 20-mesh for petrographic analysis and to minus 60-mesh for geochemical analysis. As intruded coals often contain

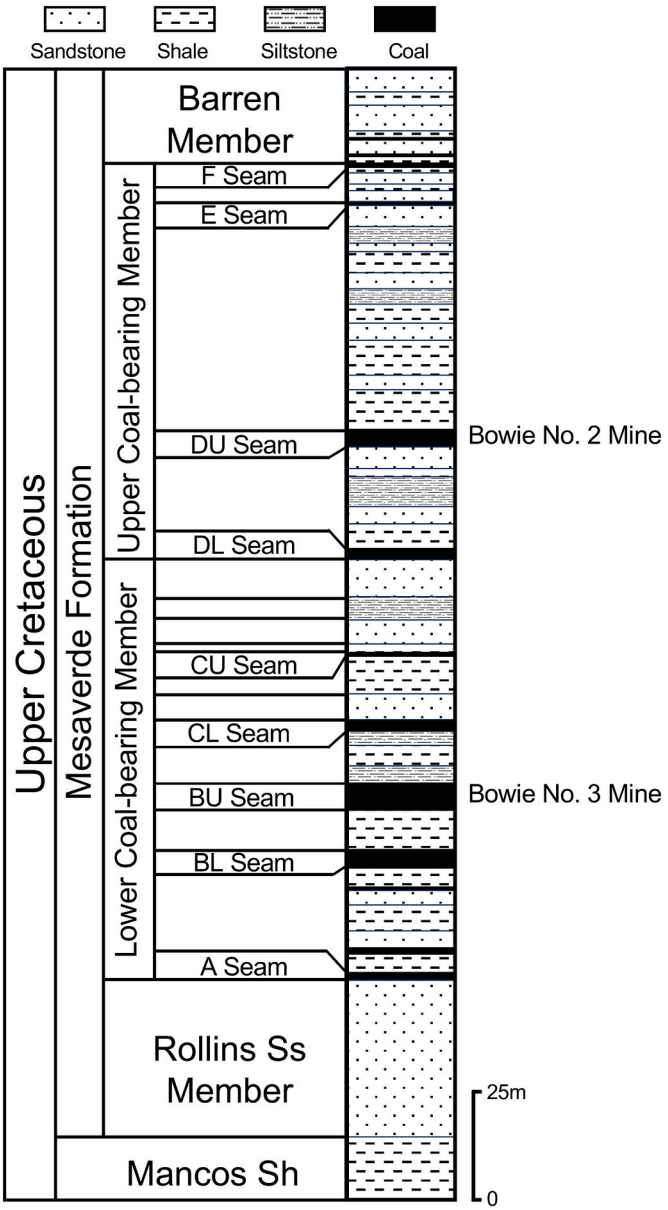

Fig. 2. Generalized stratigraphic column showing coal beds of the Mesaverde Formation at the Bowie Mine (modified from Carroll et al., 2004).

carbonates that affect the VM, carbon, and oxygen contents (e.g., Rimmer et al., 2009), all samples were treated with HCl to remove carbonate minerals prior to geochemical analysis. Approximately 3 g of each sample was treated with 35 ml 6 N HCl, allowed to react overnight, centrifuged, and filtered. This was repeated until no further effervescence was observed, at which point the samples were repeatedly washed with distilled water until a pH of 5 was attained. Select samples were inspected using reflected-light microscopy to assure the effective removal of carbonates. Proximate and ultimate analyses were then performed in compliance with standard ASTM methodologies, ASTM D3172-13 and ASTM D3176-24/ASTM D5373-21 (ASTM, 2023).

Pellets were prepared for petrographic analysis and polished to a final 0.06-μm (colloidal silica) polish according to standard procedures (Pontolillo and Stanton, 1994). Vitrinite reflectance (mean random reflectance, $\%R_r$ in oil, using non-polarized light) was measured on vitrinite macerals and their thermally altered counterparts (100 points). Analyses were performed using a Zeiss Universal reflected-light microscope equipped with a photomultiplier tube; data collection was

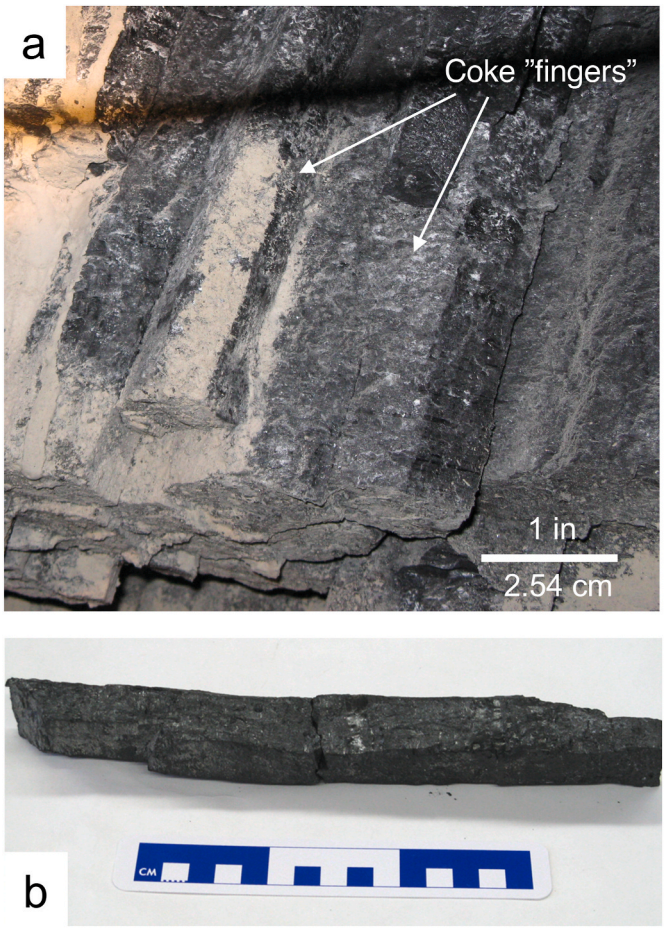

Fig. 3. Close-up of coked coal from the Bowie Mine (photo taken and samples collected near Mine Face location). a) sets of coke "fingers" about 1" (2–3 cm) in diameter and ~ 8–10" (20–25 cm) long; b) single coke "finger" - note the presence of remnant banding.

facilitated by custom computer hardware and software. Reflectance values were standardized against a SiC standard (7.45%). Typical standard deviations measured on the standard were 0.02%. Petrographic point-count analyses (500 points) were performed using a Zeiss Universal reflected-light microscope equipped with a 40x oil-immersion objective and a Swift stage. Point-count categories for all samples were as follows; vitrinite/altered vitrinite, liptinite, semi-inertinite, inertinite, and pyrolytic carbon. For reporting purposes, semi-inertinite and inertinite, were grouped together and reported as "inertinite"; pyrolytic carbon was reported separately (Table 1). Photomicrographs were taken using a Leica DM 2500P reflected-light microscope fitted with a 50x or 20x oil immersion objective under white-light illumination, using polarized light, crossed polarizers, a 1/4 λ plate, and a Lumenera Infinity 1–5C camera.

Stable carbon isotope analyses were performed at Durham University (United Kingdom) using a Thermo Delta V Advantage coupled with a Costech ECS 4010 elemental analyzer and interfaced with a Thermo-Finnigan Conflo III. Samples were decalcified prior to analysis with 3M HCl for 6 h and then rinsed to neutrality. Up to eight international and internal standards were analyzed multiple times during the generation of this isotopic dataset and analytical precision for standard $\delta^{13}C$ was 0.1‰ (2 sd.). Replicate coal analyses produced $\delta^{13}C$ values typically within 0.2‰.

3. Results

3.1. Reflectance analysis

In all transects, R_r increases towards the sills. The least mature section is the mine face suite, where R_r increases from 1.28% at the base of the seam to 2.32% directly below the intrusion (Fig. 4). In cores 1, 2, and 4 (at depth below the active mine), higher maturation levels are seen adjacent to the sills. Below the sill in core 1, R_r increases from background levels of 0.75% up to 3.17% at the sill/coal contact; directly above the sill, the reflectance is considerably higher (5.14%) and decreases from 5.14% to 3.01% furthest away from the sill (Fig. 4). Thus, reflectance is higher and decreases less above the sill; for example, over a similar distance (~1.6m) reflectance falls to 1.4% below the sill, but only to 3.01% above the sill. Below the sill in core 2, R_r decreases from 6.49% to 3.23% at a distance of ~4.3m away from a thin (~0.08m) sill. Despite the thin nature of this sill, the reflectance is much higher than that in the previous two transects. Similarly, core 4 includes a very thin sill (~0.05m), and reflectance is very high, with values increasing from 1.55% at the base of the seam to 7.01% at the sill/coal contact (Fig. 4). Above the sill, reflectance values remain high (>6%) for almost 3m before beginning to decrease, eventually reaching 4.19% at the top of the seam. Once again, above the seam the decrease in R_r is less and occurs over a greater distance.

3.2. Petrographic observations

The mine face samples are dominated by vitrinite (90–~99%) and inertinite (0–7%); the vitrinite has a higher reflectance next to the sill with that in T1 reaching >2% (Fig. 5a, Table 1). Minor amounts of incipient mosaic structure appear to have formed in some of the vitrinite (Fig. 5b and c), but most of the vitrinite shows no coke structures. However, there are also minor amounts of fine-grained to medium-grained circular mosaic coke that appear to be associated with micro fractures and veins (Fig. 5b and c). Some of this coke also contains fragments of inertinite, indicating an origin from melted coal (Fig. 5d, e, f). Whereas pronounced devolatilization vacuoles are observed within the coked fragments (Fig. 5g and h), the vitrinite shows fewer vacuoles. Note that within the mine, despite having been heated enough to form characteristic cooling features upon cooling (coke "fingers"), the coal in contact with the sill still shows normal bright banding at a megascopic scale (see Fig. 3a). No liptinites are observed due to the high level of maturation. Several occurrences of pyrolytic carbon as rims and a few masses of spherulitic pyrolytic carbon are observed, and these were associated with fragments of anisotropic coke.

In cores 1, 2, and 4, the vitrinite in the coal adjacent to each sill, has been coked and displays anisotropic, fine-grained to medium-grained circular mosaic structure and vacuoles (Fig. 5i, j, k, l). In core 1, anisotropic coke textures (primarily fine-grained circular mosaic) are visible in samples 1.7 and 1.8 above the sill (the sill lies between sample 1.8 and 1.10); sample 1.6 contains coked vitrinite with primarily incipient mosaic structure. Above sample 1.6, much of the vitrinite has formed isotropic coke with vacuoles, with some occurrences of incipient mosaic structure. Thus, anisotropic coke is seen primarily within 0.63m of the sill (equivalent to the approximate thickness of the sill, 0.62m); below the sill, these textures are observed in samples 1.10 and 1.11 within ~0.35m of the contact (or ~ 0.5x the sill thickness). Minor amounts of pyrolytic carbon are seen above the sill in samples 1.8 through 1.6, with scant occurrences towards the top of the core. Directly below the sill, sample 1.10 contains a minor amount of pyrolytic carbon but in the remaining samples little to none is seen. The pyrolytic carbon occurs mostly as thin rims along the edges of coke fragments and vacuoles. At the very base of core 1, minor amounts of liptinite (cutinite, resinite, and sporinite) are identified (Table 1). Devolatilization vacuoles are present in all samples above the sill and in the sample directly below the sill and down through 1–15. The vacuoles decrease in size and

Table 1
Petrographic and geochemical analyses of the Piceance Basin, Bowie Mine, HCl-treated coals. ID = sample identification; D = sample mid-point distance from sill, m; R_r = mean random vitrinite reflectance, % in oil; T_{peak} = estimated maximum temperature, °C, based on Barker and Pawlewicz (1994); V = vitrinite and coked vitrinite, L = liptinite, I = inertinite (excluding PC), PC = pyrolytic carbon (all on volume % basis); $\delta^{13}C$ on ‰ basis; Mois = % moisture, as received basis; Ash reported on a %, dry basis; VM (volatile matter), FC (fixed carbon), and ultimate analyses (C, H, N, S, O) reported on a % dry, ash-free (daf) basis (O by difference); Parr = mineral matter content (%, dry basis); atomic ratios O/C, H/C, and N/C calculated on a dry, mineral-matter-free (dmmf) basis.

ID	D	R_r	T_{peak}	V	L	I	PC	$\delta^{13}C$	Mois	Ash	VM	FC	C	H	N	S	O	Parr	H/C	N/C	O/C
Mine Face Samples																					
Sill (~0.5m thick)																					
T1	0.05	2.32	260	95.6	0.0	4.4	0.0	−25.26	3.50	3.54	14.35	85.65	86.85	3.22	1.95	0.60	7.38	4.15	0.442	0.019	0.058
T2	0.25	2.04	244	95.4	0.0	4.6	0.0	−25.55	3.85	2.09	15.59	84.41	88.21	3.78	1.99	0.71	5.30	2.64	0.511	0.019	0.040
T3	0.50	1.96	238	96.0	0.0	4.0	0.0	−26.29	3.75	5.42	16.84	83.16	89.01	3.94	1.93	0.64	4.48	6.19	0.527	0.019	0.031
T4	0.72	1.74	223	90.6	0.0	9.4	0.0	−25.53	3.64	7.19	18.45	81.55	89.08	4.22	1.89	0.62	4.20	8.08	0.565	0.018	0.027
T5	1.16	1.60	213	91.0	0.0	9.0	0.0	−25.51	3.58	5.28	19.41	80.59	88.22	4.18	1.81	0.61	5.17	6.02	0.565	0.018	0.037
T6	1.37	1.38	194	92.6	0.0	7.4	0.0	−25.90	3.59	5.72	23.07	76.93	86.91	4.67	1.83	0.53	6.07	6.45	0.641	0.018	0.046
T7	1.68	1.28	184	94.4	0.0	5.6	0.0	−25.53	4.01	11.44	25.00	75.00	85.43	4.87	1.83	0.52	7.36	12.61	0.680	0.018	0.053
Core 1																					
1.1	1.67	3.01	293	98.4	0.0	1.6	0.0	−25.75	2.67	3.40	10.92	89.08	90.33	3.24	1.95	0.77	3.72	4.08	0.427	0.018	0.025
1.2	1.45	3.10	297	98.6	0.0	1.4	0.0	−25.97	2.74	2.07	10.83	89.17	83.10	3.21	1.88	0.68	11.13	2.60	0.461	0.019	0.096
1.3	1.22	3.21	301	97.4	0.0	2.6	0.0	−25.31	2.78	3.37	11.09	88.91	72.87	3.08	1.64	0.68	21.73	4.01	0.505	0.019	0.217
1.4	1.01	3.20	301	99.6	0.0	0.4	0.0	−26.07	4.35	44.23	17.60	82.40	80.93	3.56	2.41	0.60	12.50	47.96	0.524	0.025	0.054
1.5	0.89	3.21	301	99.0	0.0	1.0	0.0	−25.86	5.13	54.88	21.16	78.84	84.49	4.05	2.72	0.56	8.18	59.40	0.571	0.028	−0.017
1.6	0.63	3.34	307	97.8	0.0	2.0	0.2	−25.56	5.18	4.67	12.28	87.72	90.74	2.62	2.06	0.75	3.83	5.44	0.344	0.019	0.025
1.7	0.30	3.69	319	98.4	0.0	1.2	0.4	−25.97	3.32	4.69	12.40	87.60	89.80	2.76	1.77	0.77	4.90	5.46	0.366	0.017	0.034
1.8	0.04	5.14	361	98.0	0.0	1.8	0.2	−26.37	3.37	16.48	9.30	90.70	93.24	2.45	1.64	0.40	2.28	17.98	0.313	0.015	0.004
Sill (~0.62 m thick)																					
1.10	0.12	3.17	300	99.2	0.0	0.6	0.2	−25.12	3.23	8.23	11.49	88.51	90.32	3.13	2.03	0.50	4.02	9.13	0.413	0.019	0.025
1.11	0.35	2.87	287	99.2	0.0	0.8	0.0	−25.37	3.06	6.16	11.96	88.04	89.59	3.28	2.05	0.58	4.49	6.95	0.437	0.020	0.031
1.12	0.64	2.75	282	98.6	0.0	1.4	0.0	−25.48	3.25	8.76	12.89	87.11	89.53	3.44	2.08	0.57	4.39	9.75	0.457	0.020	0.028
1.13	0.92	2.26	257	99.0	0.0	1.0	0.0	−25.72	3.70	9.95	15.33	84.67	76.55	3.25	1.75	0.52	17.94	11.00	0.505	0.020	0.165
1.14	1.01	2.05	244	98.6	0.0	1.0	0.4	−25.65	3.61	5.41	17.16	82.84	87.05	4.01	2.31	0.64	6.00	6.17	0.549	0.023	0.045
1.15	1.33	1.66	217	97.8	0.0	2.0	0.2	−25.89	3.35	4.43	20.74	79.26	88.31	4.27	2.03	0.58	4.80	5.09	0.577	0.020	0.035
1.16	1.61	1.40	195	98.6	0.0	1.4	0.0	−25.99	5.92	48.24	29.10	70.90	78.97	5.11	1.80	0.57	13.55	52.26	0.771	0.020	0.055
1.17	1.88	0.94	145	99.2	0.0	0.8	0.0	−26.16	3.68	4.79	31.21	68.79	82.99	4.97	1.80	0.64	9.59	5.51	0.714	0.019	0.080
1.18	2.09	0.75	115	97.0	2.0	1.0	0.0	−26.06	4.22	3.52	39.00	61.00	80.90	5.25	1.84	0.69	11.32	4.17	0.773	0.019	0.099
Core 2																					
Sill (~0.08 m thick)																					
2.2	0.11	6.49	391	99.0	0.0	0.0	1.0	−26.90	1.81	33.69	8.62	91.38	90.37	1.59	1.44	0.11	6.49	36.42	0.210	0.014	0.020
2.3	0.25	6.25	387	98.4	0.0	0.8	0.8	−26.53	1.70	57.74	12.47	87.53	85.10	2.01	2.18	0.10	10.61	62.38	0.282	0.022	−0.003
2.4	0.43	5.95	380	99.6	0.0	0.2	0.2	−26.36	1.89	13.99	7.57	92.43	83.15	1.20	0.83	0.09	14.73	15.16	0.172	0.009	0.121
2.5	0.62	6.22	386	99.0	0.0	0.8	0.2	−26.29	2.70	28.90	7.37	92.63	93.21	1.31	1.24	0.14	4.10	31.27	0.167	0.011	0.006
2.6	2.44	5.66	374	97.8	0.0	2.2	0.0	−26.40	3.03	11.07	5.33	94.67	95.21	1.36	1.10	0.16	2.16	12.03	0.171	0.010	0.009
2.7	2.61	5.62	373	98.4	0.0	1.6	0.0	−25.89	3.90	11.07	5.59	94.41	95.35	1.32	1.28	0.19	1.86	12.05	0.165	0.012	0.006
2.8	2.92	5.57	372	98.8	0.0	1.2	0.0	−25.98	5.08	11.61	5.73	94.27	92.31	1.24	1.31	0.41	4.74	12.74	0.160	0.012	0.028
2.9	3.15	5.45	369	99.0	0.0	1.0	0.0	−25.59	3.96	20.54	6.46	93.54	92.64	1.53	1.31	0.42	4.10	22.37	0.197	0.012	0.015
2.10	3.35	5.39	368	98.6	0.0	1.4	0.0	−26.09	3.87	16.30	7.26	92.74	92.94	1.57	1.28	0.46	3.75	17.82	0.202	0.012	0.016
2.11	3.55	4.72	351	98.4	0.0	1.6	0.0	−25.38	4.18	8.61	8.42	91.58	91.48	2.16	1.61	0.48	4.27	9.54	0.281	0.015	0.027
2.12	3.76	4.32	339	98.0	0.0	2.0	0.0	−25.96	16.57	49.68	16.36	83.64	85.40	2.39	2.21	0.95	9.05	53.92	0.333	0.022	0.006
2.13	3.96	3.61	316	97.0	0.0	3.0	0.0	−25.65	4.18	8.60	8.63	91.37	39.43	1.46	0.90	0.53	57.69	9.55	0.441	0.020	1.079
2.14	4.27	3.23	302	95.8	0.0	4.2	0.0	−26.10	4.89	11.28	8.86	91.14	92.37	2.41	1.84	0.59	2.79	12.47	0.311	0.017	0.012
Core 4																					
4.2	4.52	4.19	335	98.8	0.0	1.0	0.2	−26.03	2.05	8.99	6.66	93.34	90.92	1.99	1.12	0.21	5.75	9.82	0.261	0.011	0.040
4.3	4.29	5.18	362	99.2	0.0	0.8	0.0	−26.24	2.78	8.14	5.05	94.95	43.15	1.33	1.22	0.08	54.21	8.83	0.368	0.024	0.930

(*continued on next page*)

Table 1 (*continued*)

ID	D	R_r	T_{peak}	V	L	I	PC	$\delta^{13}C$	Mois	Ash	VM	FC	C	H	N	S	O	Parr	H/C	N/C	O/C
4.4	3.91	5.88	379	98.8	0.0	1.0	0.2	−26.24	1.91	8.16	3.69	96.31	95.19	1.33	1.12	0.16	2.20	8.89	0.166	0.010	0.011
4.5	3.31	6.55	393	98.2	0.0	1.6	0.2	−25.98	2.04	8.30	3.91	96.09	95.93	1.42	1.13	0.16	1.36	9.04	0.177	0.010	0.004
4.6	3.03	6.81	397	96.6	0.0	3.4	0.0	−26.19	1.80	9.13	4.80	95.20	87.20	1.30	0.99	0.15	10.37	9.94	0.177	0.010	0.082
4.7	2.62	7.33	407	95.6	0.0	4.0	0.4	−26.19	0.81	7.63	4.02	95.98	83.45	1.12	0.89	0.12	14.42	8.30	0.160	0.009	0.123
4.8	2.38	6.52	392	96.4	0.0	1.6	2.0	−26.59	1.20	8.61	4.76	95.24	87.98	1.18	0.97	0.13	9.73	9.37	0.160	0.009	0.076
4.9	2.20	6.75	396	97.6	0.0	2.2	0.2	−26.11	1.55	8.76	4.89	95.11	72.77	1.09	0.79	0.13	25.22	9.52	0.179	0.009	0.251
4.10	1.81	7.32	407	97.4	0.0	2.4	0.2	−26.26	0.94	9.53	5.01	94.99	81.77	1.09	0.93	0.10	16.12	10.34	0.159	0.010	0.140
4.11	1.46	6.49	391	98.8	0.0	1.2	0.0	−26.03	0.73	12.16	4.67	95.33	91.02	1.04	0.76	0.07	7.11	13.16	0.136	0.007	0.049
4.12	1.16	6.44	390	95.8	0.0	1.8	2.4	−26.04	0.87	11.30	5.61	94.39	75.29	1.01	0.61	0.09	23.00	12.25	0.160	0.007	0.219
4.13	0.86	6.64	394	95.6	0.0	1.4	3.0	−26.58	1.48	17.38	6.06	93.94	94.58	1.20	0.92	0.14	3.16	18.83	0.151	0.008	0.011
4.14	0.62	6.92	399	96.6	0.0	1.6	1.8	−26.65	1.15	12.38	5.05	94.95	83.07	1.00	0.79	0.13	15.01	13.43	0.144	0.008	0.125
4.15	0.39	6.97	400	96.2	0.0	2.8	1.0	−26.39	1.03	13.92	5.45	94.55	94.85	1.14	0.90	0.11	3.00	15.09	0.143	0.008	0.013
4.16	0.04	7.01	401	97.0	0.0	1.0	2.0	−26.10	1.71	17.38	4.99	95.01	62.68	1.13	0.83	0.14	35.23	18.83	0.214	0.011	0.401
Sill (~0.05 m thick)																					
4.17	0.01	7.00	401	97.2	0.0	1.8	1.0	−26.54	1.84	20.99	5.05	94.95	64.94	1.13	1.15	0.14	32.64	22.73	0.207	0.015	0.352
4.18	0.21	6.53	392	97.0	0.0	2.0	1.0	−26.63	2.74	36.66	9.84	90.16	91.74	2.03	1.61	0.21	4.42	39.67	0.264	0.015	−0.003
4.19	0.61	3.68	319	94.4	0.0	5.0	0.6	−25.83	2.63	36.53	9.74	90.26	92.83	3.20	2.10	0.66	1.21	39.68	0.410	0.019	−0.030
4.21	1.35	1.84	230	96.6	0.0	3.2	0.2	−25.51	3.74	6.15	16.92	83.08	89.03	3.52	2.00	0.72	4.73	7.01	0.472	0.019	0.032
4.22	1.48	1.55	208	93.6	0.0	6.2	0.2	−25.99	3.75	8.42	18.32	81.68	88.46	3.92	1.95	0.68	4.99	9.43	0.527	0.019	0.033

become less abundant with increased distance from the sill. Vacuole formation appears better developed (more abundant and larger) in altered collodetrinite than in collotelinite. Some vacuoles are partially filled with minerals, some showing rhombohedral cleavage and that have been identified as calcite. The vitrinite often shows fracturing in samples above the sill; this may be related to local faulting and cleat formation, or to the very rapid heating experienced by the coal at the time of intrusion.

Transects from cores 2 and 4 are quite different than the previous two transects due to the very high level of maturation attained (up to ~7% R_r). In core 2, where samples are only available below the thin (0.08m) sill, the vitrinite has been coked to produce primarily fine-grained circular mosaic structure, much of which contains abundant vacuoles. Additionally, minor amounts of isotropic, incipient, and medium-grained circular mosaic coke are observed. The primary type of coke changes with increased depth below the sill, with incipient coke becoming the dominant form by sample 2.10 and then normal (high reflectance and bireflectance) vitrinite becoming dominant in sample 2.11 and the remaining samples. Most of the vitrinite shows little to no vacuole development. Throughout these lower samples, trace amounts of vesiculated coke with fine-grained circular mosaic structure co-occur. Pyrolytic carbon occurs as rims (Fig. 6a, b, c, d), spherulites (Fig. 6a, b, c, d), and botryoidal aggregates (Fig. 6e and f) in samples close to the sill (e.g., sample 2.2 contains 1.0%). The pyrolytic carbon typically occurs as ribbon-like veins within macerals, as linings along maceral edges, within devolatilization vacuoles, sometimes completely infilling the vacuoles, in spheres ranging from >1 to <20 μm in diameter, and in masses of spheres (<100 to 100–200 μm across). Pyrolytic carbon decreases with increasing distance away from the sill, with little to none occurring in those samples below sample 2.8. What few examples occur at depth are associated with rare occurrences of vesiculated coke that may be present as a contaminant or fracture fills. Samples closer to the sill also show mineral veins in association with the coked fragments.

In core 4, the availability of samples both above and below the sill at one location allow a more direct comparison of features. Below the sill, the maturation level drops off very quickly. In sample 14.17, directly below the sill, vitrinite has been coked, showing primarily fine-grained circular mosaic structure with abundant vesicles. Minor amounts of incipient coke are also observed. Throughout the sample, pyrolytic carbon occurs as spherulites in vacuoles, mineral veins, or as large masses, along with rims and botryoidal masses. Directly below this sample (only 0.2m below the sill) there is much less fine-grained coke and more incipient coke; some of the altered vitrinite occurs as vesiculated isotropic coke rather than an anisotropic form, a trend that continues into the underlying samples where most of the altered vitrinite occurs as vesiculated isotropic coke (again the vacuoles are more well developed in the altered collodetrinite than in collotelinite) with only minor amounts of fine-grained circular mosaic coke. Pyrolytic carbon is common (as rims) in 4.18, but decreases in the underlying samples. The bottom two samples of the transect are primarily high reflectance vitrinite, most of which is not vesiculated. Some pieces of fine-grained, vesiculated coke occur, some associated with mineral veins. Above the sill in core 4, maturation levels do not drop off significantly until close to the top of the section; for example, values close to and even above 7% are still seen over 3m above the 0.5m-thick sill, and the petrography reflects this high level of maturation. All samples above the sill contain coke with mostly fine-grained circular mosaic structure, high degrees of vesiculation, and pyrolytic carbon. Typically, samples contain a variety of textures including incipient, fine-grained circular, medium-grained circular, and fine-grained lenticular mosaic structures. Overall, core 4 has the highest pyrolytic carbon contents, including rims, spherulites (sometimes in large masses, other times in vacuoles), and botryoidal forms. The amount of pyrolytic carbon generally is lower towards the top of the core, with increased amounts close to the sill.

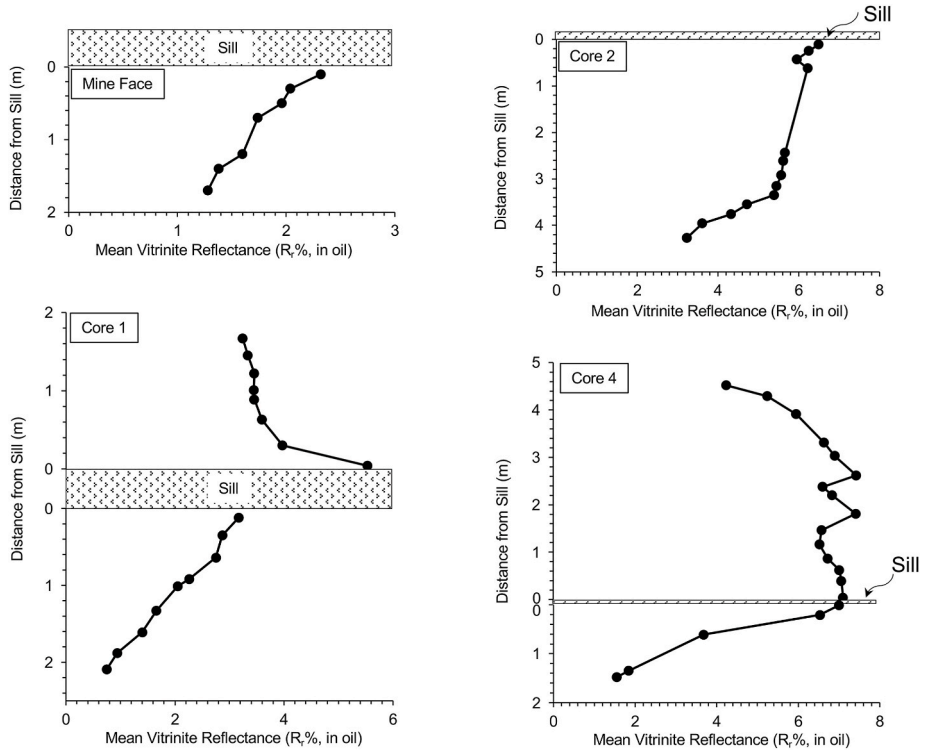

Fig. 4. Vitrinite reflectance trends for the mine face and core sample suites. Approximate sill thicknesses represented.

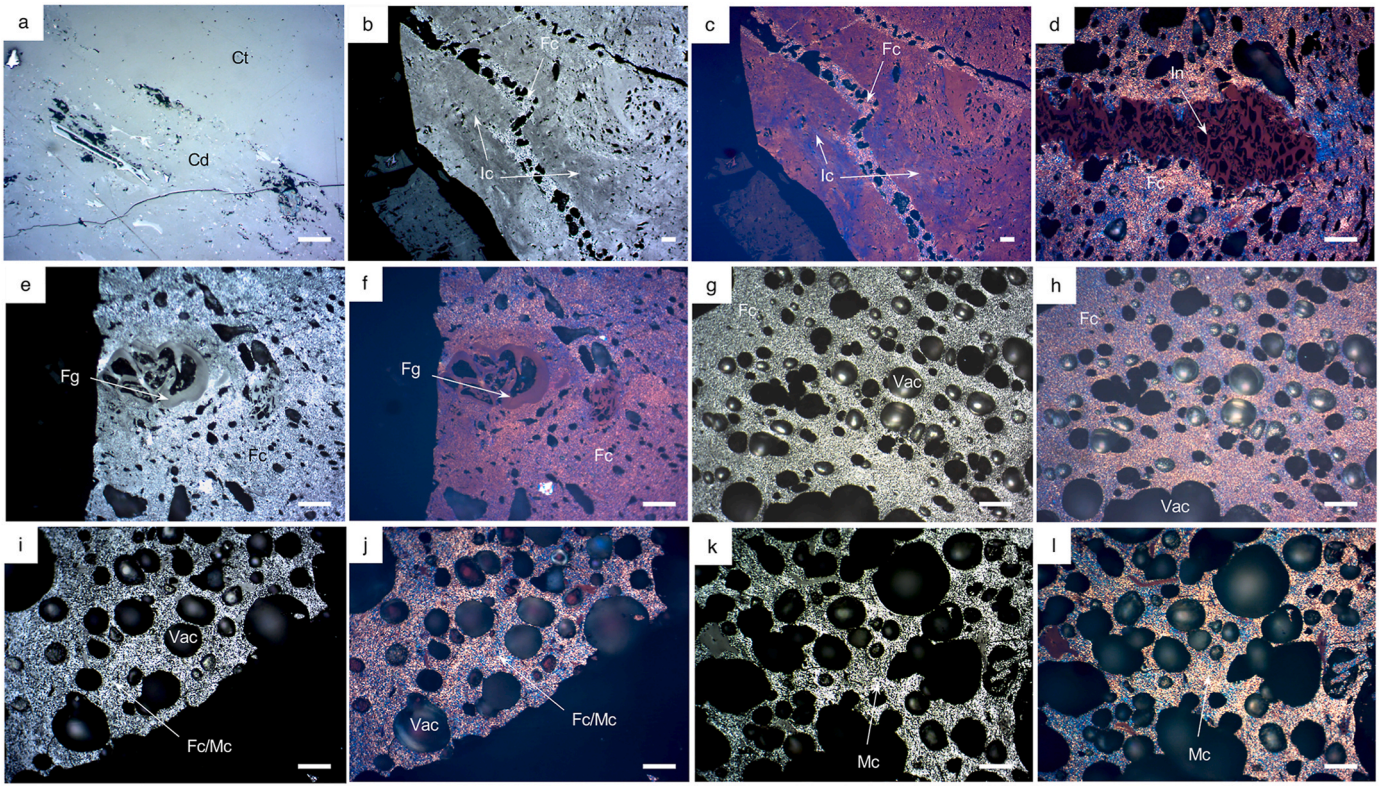

Fig. 5. Photomicrographs showing altered and coked coal. a). High reflecting vitrinite (collodetrinite (Cd) and collotelinite (Ct)) showing no evidence of coking, directly beneath the sill at the mine face (T1, R_r = 2.32%) (polarized white light); b) fragments showing incipient mosaic structure (Ic) with fractures filled with devolatilized fine-grained circular mosaic (Fc) (T1, R_r = 2.32%) (partially crossed polarizers, 20x objective); c) same field of view as (b) (crossed polarizers and 1/4 λ plate, 20x objective); d) fine-grained circular mosaic texture (Fc) with inertinite (In) (T1, R_r = 2.32%) (crossed polarizers and 1/4 λ plate); e) fine-grained circular mosaic (Fc) with isotropic funginite (Fg) (T5, R_r = 1.60%) (partially crossed polarizers); f) same field of view as (e) (crossed polarizers and 1/4 λ plate); g) fine-grained circular mosaic (Fc) with abundant vacuoles (Vac) (T7, R_r = 1.28%) (partially crossed polarizers); h) same field of view as (g) (crossed polarizers and 1/4 λ plate); i) fine to medium-grained circular mosaic (Fc/Mc) with abundant vacuoles (Vac) (4.4, R_r = 5.88%) (partially crossed polarizers); j) same field of view as (i) (crossed polarizers and 1/4 λ plate); k) medium-grained circular mosaic (Mc) (4.3, R_r = 5.18%) (partially crossed polarizers); l) same field of view as (k) (crossed polarizers and 1/4 λ plate). All photos taken using a 50x oil objective, except where noted. Scale bar = 20 μm.

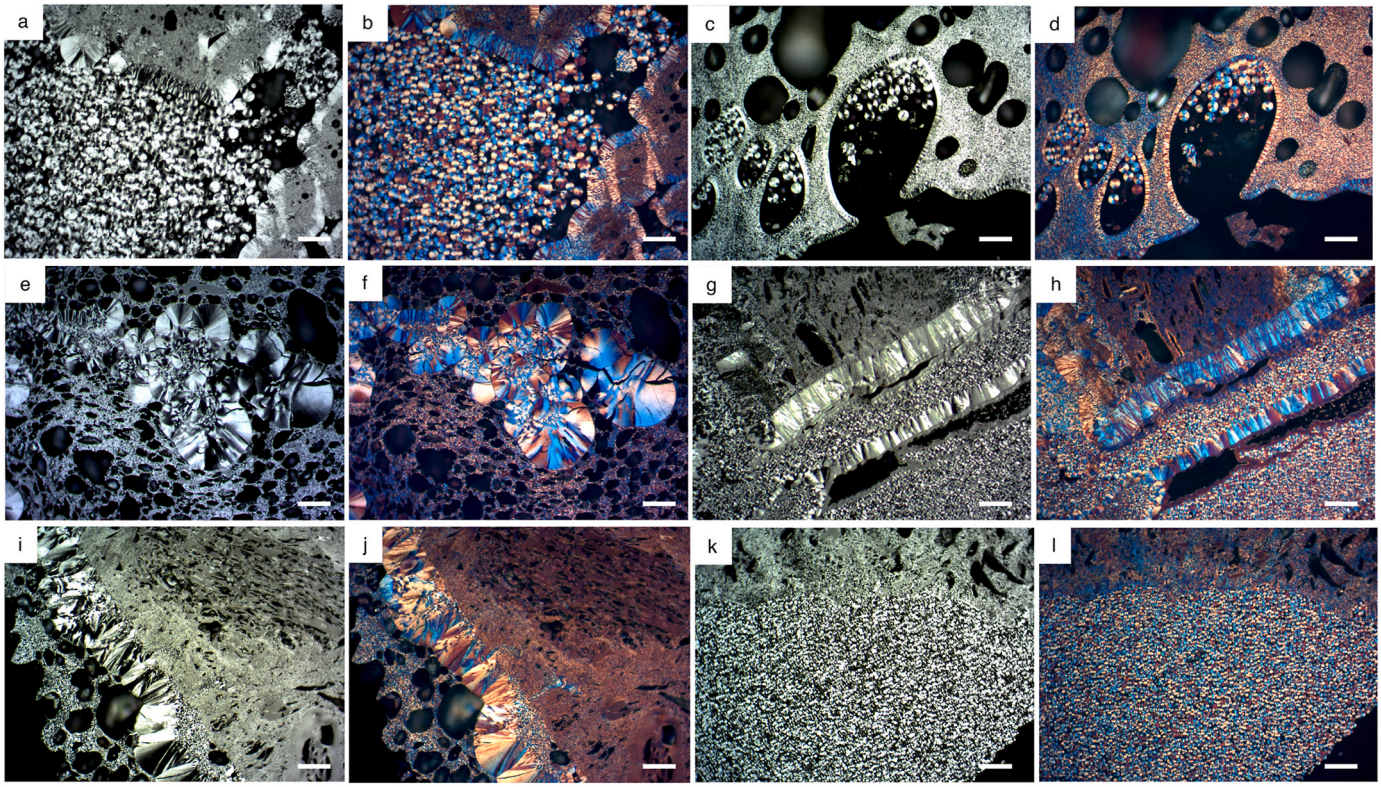

Fig. 6. Photomicrographs showing occurrences of pyrolytic carbon. a). Rims and spherulites of pyrolytic carbon (2.4, R_r = 5.95%) (partially crossed polarizers); b) same field of view as (a) (crossed polarizers and 1/4 λ plate); c) rims and spherulites of pyrolytic carbon (2.4, R_r = 5.95%) (partially crossed polarizers); d) same field of view as (c) (crossed polarizers and 1/4 λ plate); e) botryoidal pyrolytic carbon in mass of fine-grained circular mosaic coke (2.4, R_r = 5.95%) (partially crossed polarizers); f) same field of view as (e) (crossed polarizers and 1/4 λ plate); g) rims, botryoidal, and spherulitic forms of pyrolytic carbon (4.8, R_r = 6.52%) (partially crossed polarizers); h) same field of view as (g) (crossed polarizers and 1/4 λ plate); i) rim of pyrolytic carbon separating two types of coke (4.10, R_r = 7.32%) (partially crossed polarizers); j) same field of view as (i) (crossed polarizers and 1/4 λ plate); k) mass of spherulitic pyrolytic carbon (4.17, R_r = 7.00%) (partially crossed polarizers); l) same field of view as (k) (crossed polarizers and 1/4 λ plate). All photos taken using a 50x oil objective. Scale bar = 20 μm.

3.3. Ultimate and proximate analysis

In most of the transects studied, below the sills VM (wt% dry, ash-free (daf) basis, HCl-treated) decreases towards each sill, with the exception of core 2; above the sills (cores 1 and 4), there is no clear increase in VM away from the intrusion (Table 1, Fig. 7). This is due to the very high level of alteration seen above the sills. The least altered coals in these sections are seen at the bottom of core 1, where VM is 39%. Approaching the sills from below, VM decreases from 25% to 12–14% in the mine face transect and from 39% to ~12% in core 1; beneath the sills in cores 2 and 4, VM is lower overall, reaching ~7–8% and ~5% directly beneath the sill, respectively. Above the sill, in cores 1 and 4, there is little regular change in VM. Within the transects, marked increases in VM content appear to coincide with increases in ash yield (Table 1, Fig. 7). Note that these samples have been treated with HCl to remove carbonates (which can interfere with VM analyses), so the inorganics would only include very minor amounts of carbonate and mostly silicate minerals, probably quartz and clays. Based on the low sulfur content of these samples (<0.8%), only minor amounts of pyrite are present. Ash yields range from 2.1% to 57.7% (dry basis). The majority of samples (46 samples or 81%) contain <20% ash; samples with ash yields >20% (9 samples) are those that affect the VM analyses the most (Fig. 7). Moisture content (as determined basis) generally decreases with increasing reflectance; however, there is considerable scatter in the data (Table 1).

Even after recalculation to a daf basis, the ultimate analyses are affected by the high ash yields (Table 1). One factor is the loss of structural water in clays that affects the H contents of the organic fraction, and the breakdown of any remaining carbonates that affect the C and O contents (Given and Yarzab, 1978). As O is calculated by difference, any mineral effect on C, H, N, or S will impact reported O contents. Use of dry, mineral-matter-free (dmmf) data (which uses the Parr formula to calculate mineral matter) attempts to account for the loss of water of decomposition in clays at high temperatures in the ultimate analytical method and thus incorporates less error than when dry, ash-free data are used (Given and Yarzab, 1978). This is in addition to the correction for the H contribution from free moisture that is made in the calculation of H on a dry basis (ASTM D3180-15, ASTM, 2023). The Parr formula is MM = 1.08 Ash +0.55 S, where MM is mineral matter, and S is total sulfur (all parameters on a dry basis) (ASTM D388-23, ASTM, 2023).

Due to the influence of mineral matter on VM and ultimate components, the best assessment of trends approaching the sills is the evaluation of atomic ratios for the coals, especially H/C (calculated on a dmmf basis, Table 1). The H/C for samples beneath the sill in the mine face samples and cores 1 and 4, shows a consistent decrease approaching the sill (Fig. 8). A less consistent decrease in H/C is seen above the sill in core 1. Below core 2 and above core 4, however, a clear trend is not seen as the H/C is already low (~0.2); note that these samples have very high reflectances (R_r mostly >4%). Further clarification of trends is possible by examining data for low-ash samples (<20% ash, dry basis). As shown in Fig. 9, in low-ash samples there is a very clear relationship between decreasing H/C (dmmf) and decreasing VM (daf), and decreasing H/C (dmmf) and increasing R_r (%, in oil) for coals below the sills. Above the sills, the trends are less clear, with the VM contents and H/C ratios remaining low. It is clear that H/C decreases with increased rank,

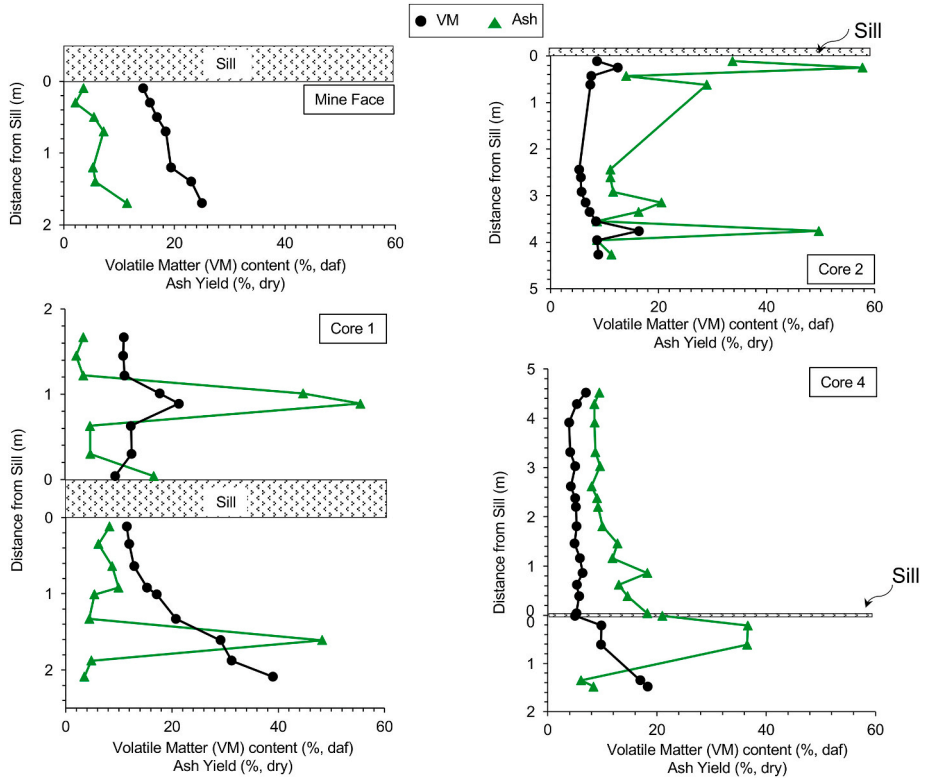

Fig. 7. Variations in volatile matter content (%, daf) and ash yield (%, dry) for HCl-treated samples in relation to sills.

whether measured by VM or R_r, and that, in general, the trends are more pronounced below the sills than above. Above the sills, rank remains higher for greater distances and is reflected in the geochemical composition.

3.4. Stable carbon isotope analyses

The relationship between distance from the sills (and thus rank) and $\delta^{13}C$ is not clear (Fig. 10). No trend is seen below the sill in the mine face samples; however, a shift to less negative values is seen below the sill in core 1. In this core, the greatest change in R_r (%) is observed (0.75–3.2%) beneath the sill, and across this rank difference $\delta^{13}C$ changes from −26.1% to −25.1‰. This small, but significant change in $\delta^{13}C$ correlates significantly with rank increase (Fig. 11) (r = 0.97). However, no clear relationships are observed above the sill. In cores 2 and 4 (the higher rank transects with R_r generally >4%), there is a small shift (~0.6–1‰) towards more depleted values directly beneath the sills (Fig. 10). Beyond this, both show some variability in $\delta^{13}C$ but no specific trends. Cores 2 and 4 are the highest rank transects and more consistently contain pyrolytic carbon. A comparison of $\delta^{13}C$ values and petrographic composition (see Table 1, Fig. 10) suggests that $\delta^{13}C$ shifts to more negative values in those samples that contain small amounts of pyrolytic carbon, particularly those from cores 2 and 4.

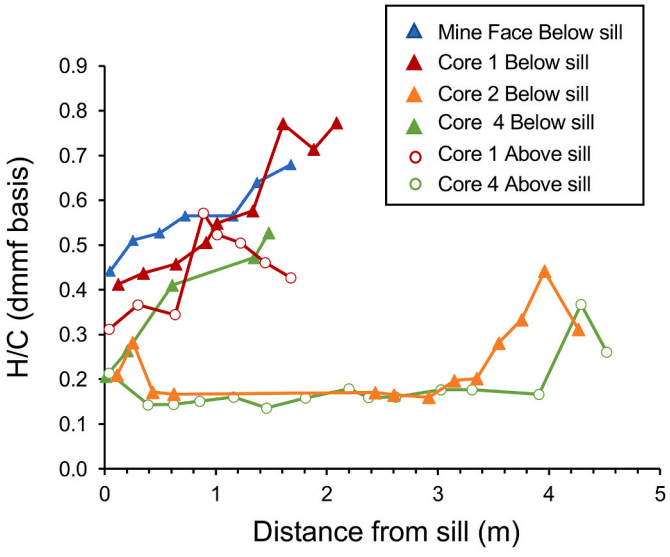

Fig. 8. H/C (dmmf basis) vs. distance from sills.

4. Discussion

4.1. Effects of contact metamorphism

The lowest reflectance values measured in any of the coal samples is 0.75% (at the base of core 1). All other sample suites have profiles that start at considerably higher reflectance levels (~1.3% for the mine face samples, 3.2% for core 2, and 1.5% for core 4), hence the apparent absence of liptinite (which is no longer distinguishable at these vitrinite reflectance levels). A background reflectance of 0.75% for the region indicates a coal rank of high volatile A bituminous, which would be consistent with rank observations for the region (high volatile A and B bituminous) (Goolsby et al., 1979; Johnson and Nuccio, 1986; Hettinger et al., 2000), but slightly higher than the inferred rank from analytical data for the Bowie Mine (high volatile C or B bituminous) presented in Carroll (2005) and Carroll and Widmann (2000). Hettinger et al. (2000) reported that coals along the southern flank of the Piceance Basin range from high A to B volatile bituminous, with coal rank increasing towards the southeast, with some beds reaching low volatile bituminous, semi-anthracite, and anthracite in the Crested Butte field. A vitrinite reflectance of 0.75% would suggest exposure to burial temperatures of ~112 °C, based on relationships established for normal burial maturation ($T_{peak} = (\ln(R_r)+1.68)/0.0124$) (Barker and Pawlewicz, 1994).

All four coal transects studied show the effects of contact

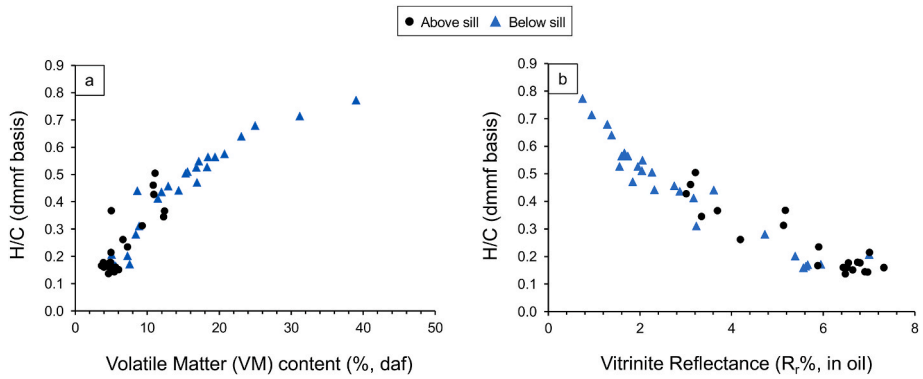

Fig. 9. Variations in geochemical composition for low-ash (<20%, dry basis) samples above and below sills. a) H/C (dmmf basis) vs. VM (daf basis); b) H/C (dmmf basis) vs. R_r (%, in oil).

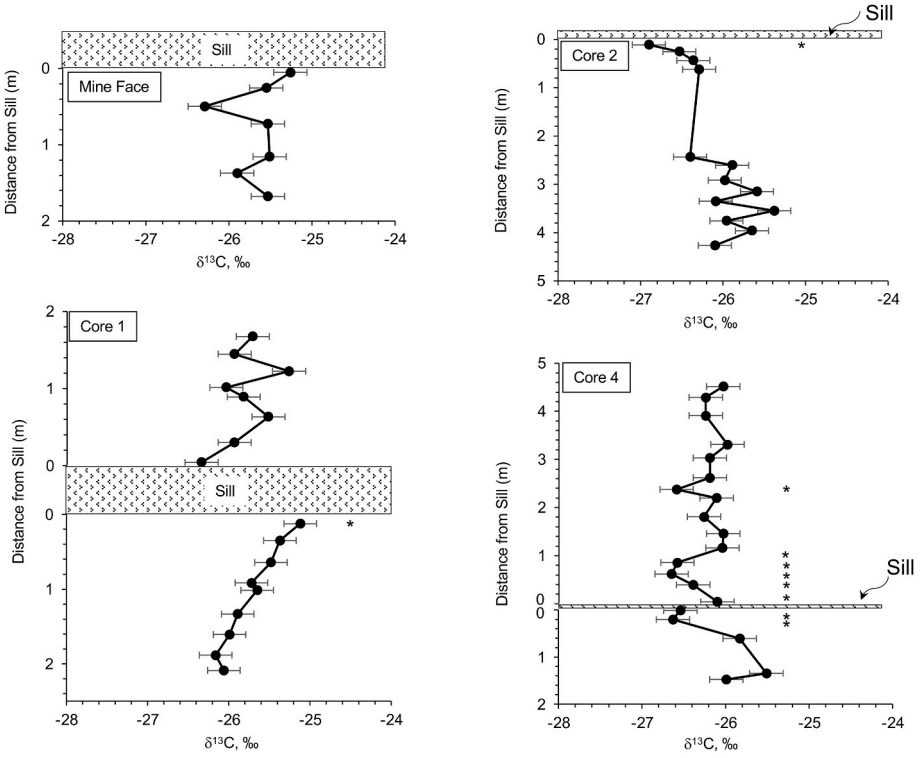

Fig. 10. Variations in $\delta^{13}C$ (‰) vs. distance from sills. Bars indicate ±0.2‰ analytical error. * indicates samples with >1% pyrolytic carbon.

metamorphism due to the emplacement of the sills. Adjacent to each sill, zones of altered coal are observed; approaching each sill, coals show increased reflectance, coked vitrinite, abundant devolatilization vacuoles, loss of ability to identify liptinite macerals, and accumulations of pyrolytic carbon (in the most altered transects), accompanied by geochemical changes that include a decrease in VM and the H/C ratio. In the mine, the presence of coked coal "fingers" beneath the sill was also observed (Fig. 3) and several of the cores included intervals of coke "fingers". Vitrinite reflectance increases from a background high volatile A bituminous level (R_r = ~0.75%) to anthracite/meta-anthracite levels and coke (in excess of 6% or 7% in some cases) in the most highly altered coal adjacent to the sill contacts (Table 1, Fig. 4). Even though these sills are relatively thin (0.05–0.62m), coal alteration is extensive. If it is assumed that ~0.75% is the background maturation level, as seen at the base of core 1, the alteration halo below this sill is ~3.4x the sill thickness. In the other transects, none of the reflectance values return to background levels within the distances sampled. Due to the extensive alteration halos, it is difficult to measure their average magnitude from the Bowie Mine samples. The size of the contact aureole has been shown to be greater above sills than below in a study of intrusions in the Gunnedah Basin, Australia (Gurba and Weber, 2001), and that appears to be the case here for cores 1 and 4 where sampling incorporated coals both above and below the sills (Fig. 4). The overall very high reflectance levels observed in cores 2 and 4 (R_r = ~4–6%) suggest very extensive alteration above background levels despite the very thin nature of the sills seen in the cores. It is possible that additional sills not observed in the cored intervals may be present locally, that large volumes of magma may have travelled along these sills for extended periods, and/or that hot fluids were transported along fractures. The latter may be responsible, in particular, for the irregular reflectance profile seen above the sill in core 4 as suggested for other intruded coals (e.g., Rimmer et al., 2009; Presswood et al., 2016; Moroeng, 2022), and indeed there is evidence of extensive fracturing and mineralization within the cores. For the Bowie Mine, Robeck (2005) suggested significant migration of hydrothermal waters occurred along faults and fracture systems within the mine, also noting that the combination of hydrothermal fluids and gases

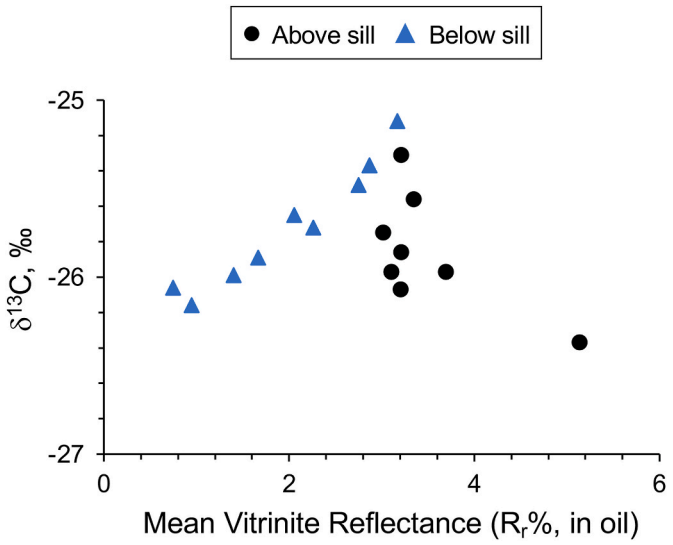

Fig. 11. Relationship between R_r (%, in oil) and $\delta^{13}C$ (‰) in core 1.

from the devolatilizing coal associated with sill intrusion could have resulted in high pore fluid and gas pressures, producing new fracture networks. The sills in the transects at depth below the mine (where cores 1, 2, and 4 were collected) may have experienced continued magma flow over longer periods of time, devolatilizing large volumes of coal as a result of a long-term source of heat.

The observed anisotropic coke textures provide additional clues to rank at the time of intrusion. The presence of incipient and fine-to medium-grained circular mosaic coke texture (Fig. 5) suggests a pre-intrusion rank of high volatile A bituminous, and a reflectance of approximately 0.8–1.0% R_r. As the background reflectance levels suggested by core 1 are 0.75% R_r, this coke texture would suggest that the coal at the time of intrusion was close to its modern-day rank, confirming earlier estimates by Johnson and Nuccio (1986) and Robeck (2005). Notably, the observed coke texture suggests a slightly higher rank at the time of intrusion than would be anticipated based solely on a comparison to commercial metallurgical coke textures. Based on the current study and previous results, the difference appears to be on the order of 0.1–0.2% R_r. A similar disparity between coke textures and background coal reflectance levels was reported by Amijaya and Littke (2006) and Rahman and Rimmer (2014). This might be expected as the rate and duration of heating, maximum temperatures attained, pressure conditions, and fluid conditions would be quite different (and unknown) in the formation of natural coke. For example, enhanced anisotropy could result due to higher pressures (Goodarzi, 1985a; Murchison, 2006), higher temperatures (Chaudhuri et al., 1997), or higher heating rates (Goodarzi and Murchison, 1978). Alternatively, the coal may have experienced two phases of heating or some "pre-heating" just prior to the time of intrusion that could have increased rank locally (Amijaya and Littke, 2006; Rahman and Rimmer, 2014).

Of additional interest is the presence of multiple populations of coke type within individual samples; some samples contain a mix of altered vitrinite of anthracitic reflectance level, incipient coke, and anisotropic coke with fine-grained to medium-grained circular mosaic structure. In some less thermally altered samples, the co-occurrence of vitrinite and minor amounts of coke (<1–2%) may have resulted from migration of fluidized coal along fractures into less altered parts of the seam; similarly in more altered coals, the presence of different coke textures could reflect an influx of melted coal at different times. Macroscopically, there is abundant evidence of fractures within the cores, which would help explain the mixed coke types observed. Movement of superheated fluids along fractures could also have led to additional alteration (e.g., Hower et al., 2019, 2021; Wang et al., 2024). In the higher rank samples, pyrolytic carbon is often associated with mineral veins. These observations suggest multiple episodes in the epigenesis of the coke and pyrolytic carbon features. While it is not possible to rule out minor cross contamination of the samples in the core boxes, the fact that many sampled intervals were coherent allows confidence in the integrity of the samples, and the presence of fractures throughout the cores and the ubiquitous presence of multiple phases suggests that this mostly likely reflects a natural heterogeneity within the samples.

4.2. *Pyrolytic carbon occurrence associated with intruded coal*

Pyrolytic carbon is often observed in natural coke and forms from the cracking of the gas phase during thermal alteration of coals by igneous intrusions (Taylor et al., 1998; Kwiecińska and Petersen, 2004; Kwiecińska and Pusz, 2016). As these gases migrate through the coal, they can re-deposit as pyrolytic carbon upon cooling. Pyrolytic carbon has been reported in intruded coals both above and below sills in the Gunnedah Basin, Australia (Gurba and Weber, 2001), adjacent to a sill in the Bowen Basin (Kisch and Taylor, 1966), associated with both dikes and sills (the latter more so) in the Raton Basin (Cooper et al., 2007; Rimmer et al., 2015), as well as in intruded coals in Canada (Goodarzi, 1985b), Antarctica (Schapiro and Gray, 1966; Sanders and Rimmer, 2020), India (Singh et al., 2007, 2013), South Africa (Falcon and Snyman, 1986), and China (Li et al., 2018; Wang et al., 2019), among others. This newly-formed, vapor-deposited material can occur as spheres (spherulitic pyrolytic carbon), botryoidal aggregates (concentrically spherical structures referred to as "cone-in-cone" structures), ribbon-like fracture fill, vacuole fill, and thin layers along coked surfaces (Goodarzi et al., 1992; Rimmer et al., 2015; Kwiecińska and Pusz, 2016); all of these forms are seen in the Piceance Basin samples (Fig. 6). Pyrolytic carbon is often, but not universally, anisotropic (Kwiecińska and Pusz, 2016) and its presence suggests temperatures of at least 500 °C (Goodarzi et al., 1993) or 600 °C (Chandra and Taylor, 1982). The type of pyrolytic carbon may be dependent on temperatures of formation: spherulitic pyrolytic carbon forms rapidly and at higher temperatures than laminar accumulations that form over time from successive generations of gas (Goodarzi, 1985b).

In the Piceance Basin cores, the decrease in VM (Fig. 7), decrease in H/C (Fig. 8), widespread occurrence of devolatilization vacuoles in the contact aureoles, and reported loss of coal volume in the study area (Robeck, 2005) provide ample evidence for extensive loss of volatiles by the coal due to intrusion by the sills. Because the sills run along the coal seams, instead of cross cutting as would be the case for dikes, a significant volume of coal was affected. It is apparent that at very high ranks, especially >4% R_r, some of the volatiles re-condensed as pyrolytic carbon along fractures and in vacuoles (Fig. 6). This is particularly prevalent adjacent to the sills, but also occurs away from the sills (but still within the contact aureole) suggesting some outward migration of these gases. Multiple layers and forms of the pyrolytic carbon suggests several episodes of volatile formation and condensation occurred.

The presence of pyrolytic carbon provides another indication of the temperatures experienced by the intruded coal. As a first estimation, the maximum temperature experienced by the coals can be estimated by the relationship developed for hydrothermal conditions by Barker and Pawlewicz (1994): $T_{peak} = (\ln(R_r)+1.19)/0.00782$ where T_{peak} = maximum temperature (°C) attained and R_r = random vitrinite reflectance (%, in oil). Based on fluid inclusion data, this geothermometer is thought to be valid up to ~300 °C (or R_r ~ 3.2%); above that level, the relationship may underestimate temperatures (Barker et al., 1998). Based on this geothermometer, maximum temperatures experienced by the coal in the mine face reached 260 °C and 300 °C beneath the sill in core 1 (Table 1). Above the sill in core 1, temperatures may have been as high as 360 °C and only decreased to ~290 °C away from the sill; beneath the sill, temperature decreased to 115 °C. According to this approach, cores 2 and 4 generally experienced much higher temperatures, >300 °C and as high as 400 °C at the sill contact; for these two

cores, the lowest temperatures are seen at the bottom of core 4 which may have only reached ~200 °C in the sample furthest away from the sill (Table 1). As these estimates are less reliable at higher temperatures, other approaches can help refine the heating conditions. The presence of anisotropic mosaic textures in the coke indicates melting and resolidification of the coal. In the laboratory and in commercial coke manufacture, these processes occur at temperatures of ~350–450 °C and ~450–500 °C, respectively (Crelling, 2008). Other authors have suggested slightly higher temperatures for mosaic formation, 460–470 °C (Brooks and Taylor, 1968) and 480–490 °C (Taylor, 1961). A coal-sill contact temperature ($T_{contact}$) of ~650 °C would be suggested by the relationship of Carslaw and Jaeger (1959): $T_{contact} = (T_{magma} + T_{host})/2$ where T_{magma} and T_{host} are the initial temperature of the basaltic magma of the sill (1200 °C) and host rock (coal) (112 °C), respectively, although such temperature differences would be quite transient with rapid heating of the coal and cooling of the magma. It has been suggested that this relationship may overestimate temperatures, perhaps by as much as 200 °C (Wang et al., 2008). However, the presence of pyrolytic carbon, especially the spherulitic form, may suggests temperatures for cores 2 and 4 as high as 500–600 °C based on the work of Chandra and Taylor (1982), Goodarzi, 1985b, and Goodarzi et al. (1993).

4.3. Trends in $\delta^{13}C$

Carbon isotopic ratios for coal typically range between −22‰ and −27‰ (Whiticar, 1996). Variability in $\delta^{13}C$ may reflect the maceral composition of the coal: inertinites (or more refractory material) are isotopically heavier (enriched), liptinites are lighter (depleted), with vitrinite in between (Whiticar, 1996; Rimmer et al., 2006). As rank increases, small changes in $\delta^{13}C$ are seen at low rank, but significant changes can be observed at high levels of maturation (McKirdy and Powell, 1974; Hoefs and Frey, 1976; Whiticar, 1996). Minor changes (~1‰) have been reported for liptinites and vitrinites between 0.6% and 1.3% R_r (Whiticar, 1996) and whole coals between 0.5 and 1.7% R_r (Mastalerz and Schimmelman (2002); Boudou et al. (1984) report an enrichment of 2‰ between 0.5 and 2.0% R_r. For metamorphosed OM, $\delta^{13}C$ values of −10 to −15‰ have been reported (Hoefs and Frey, 1976). During earlier coal maturation (VM content between 40% and 20%), approximately equal amounts of CO_2 and CH_4 are released; at anthracite rank and beyond, significant amounts of CH_4 are released (Jüntgen and Karweil, 1966; Hunt, 1996). Methane shows considerable depletion (25‰) compared to the coal as it contains more ^{12}C than ^{13}C (Hoefs and Frey, 1976; Sackett, 1978). Hence, below 100–150 °C little change in coal $\delta^{13}C$ would be expected; above 200 °C ($R_r \geq 2.2\%$), coal $\delta^{13}C$ should become enriched (Hoefs and Frey, 1976). However, other work has suggested only minor changes would occur during CH_4 formation, on the order of a few per mil differences (−2 to +3.9‰) (Chung and Sackett, 1979). The degree of openness of the coal system plays a significant role in this, with very little isotopic change occurring in a semi-closed system, whereas significant enrichment (up to ~10‰) can be recorded in an open system (Ciesielczuk et al., 2021).

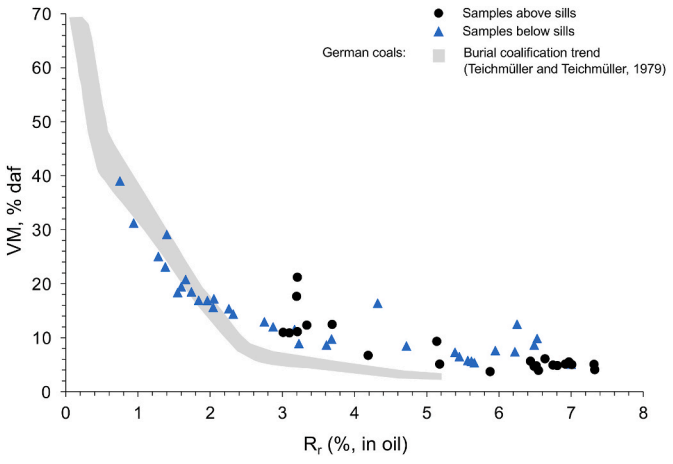

Fig. 12. Relationship between volatile matter content and random vitrinite reflectance for samples collected above and below sills.

Previous studies of intruded coals have shown that trends in $\delta^{13}C$ are ambiguous, and often sinusoidal (e.g., Cooper et al., 2007; Gröcke et al., 2009; Schimmelmann et al., 2009; Yoksoulian et al., 2016; Rahman et al., 2017) (See Fig. 12 in Sanders et al. (2023) for a compilation of trends). The Bowie Mine transects can be divided into two groups: a) below the sill in the mine face and core 1 samples that have lower reflectances, and b) above the sill in core 1 and all of cores 2 and 4 where most, if not all, of the samples have R_r >2% and as high as 7%. Although little change in $\delta^{13}C$ is seen in the mine face samples, core 1 shows a 1‰ shift to less negative values beneath the sill (Figs. 10 and 11). The samples below the sill in core 1 also show a wide range in R_r values (0.75–3.17%) across the threshold temperature (200 °C) where a shift in $\delta^{13}C$ would be anticipated. Above the sill in core 1 and in cores 2 and 4, most samples (all but two at the base of core 4) have reflectance values that suggest temperatures as high as 400 °C. The actual temperatures associated with these two cores (see discussion above) were probably much higher, as much as 500°or 600 °C (if the temperature of formation of pyrolytic carbon is considered). However, none of these samples show distinct trends in $\delta^{13}C$. At these temperatures and levels of maturation, one would expect to see considerably less negative $\delta^{13}C$ (e.g., −10 to −15‰) if the changes were to follow those seen under normal burial metamorphic conditions (such as those described by Hoefs and Frey, 1976), yet values still hover around −26‰, much like the least altered coal. One possible reason for the discrepancy is the size of the carbon reservoir. The samples studied by Hoefs and Frey (1976) were low-carbon samples (<3% organic carbon), whereas the samples here are considered coals primarily with high carbon contents (Table 1). Is it possible that the limited change in $\delta^{13}C$ could be due, in part, to the large size of the carbon reservoir (Whiticar, 1996; Sanders et al., 2023)?

Schimmelman et al. (2009) describe isotopic trends in C, N, and H adjacent to a dike in southern Illinois (USA). They suggest the observed sinusoidal trend in $\delta^{13}C$ was due to pyrolysis of organics and inorganics adjacent to the dike, transport of volatiles away from the dike, and reaction of the volatiles with slightly cooler coal away from the dike. They furthermore suggest that the system was fairly open, and fluids and volatiles could move freely through the coal seam. However, there is also some suggestion in other cases of intruded coals, that the system is less than open and that high pressures associated with the intrusion could limit the release of volatiles (Crelling and Dutcher, 1968; Podwysocki and Dutcher, 1971). Thus, it is entirely possible that the system behaved more like a semi-closed environment. Schimmelmann et al. (2009) suggest that the rapid and intense heating associated with an intrusion event is more comparable to artificial maturation rather than to normal burial maturation. Their own 5-yr artificial maturation experiments did not show a significant change in $\delta^{13}C$ (only showing a difference of 0.3‰); however, as they note, they were dealing with sealed quartz ampoules, representing a closed system in which liberated products could react with the residual kerogen (Schimmelmann et al. (2009). Other laboratory heating studies show very little isotopic fractionation in coals heated under semi-closed conditions, whereas significant enrichment $\delta^{13}C$ is seen in coals heated in an open system Ciesielczuk et al. (2021). The change in $\delta^{13}C$ in an open system can be attributed to the escape of isotopically depleted n-alkanes, expulsion of CH_4, and oxidation of ^{12}C to CO_2 (Ciesielczuk et al., 2021). This raises the possibility that the lack of clear $\delta^{13}C$ trends observed in intruded coals may be due, in part, to the semi-closed nature of the systems and that the degree of isotopic fractionation under contact metamorphic conditions may be considerably less seen than that observed under normal burial maturation conditions.

Open-system pyrolysis allows collection of gases during heating and

suggests that the $\delta^{13}C$ of generated CH_4 is temperature dependent. Berner et al. (1995) measured $\delta^{13}C$ of CH_4 generated from immature woody tissue (xylite) and kukersite (derived from extinct marine algae, *Gloecapsomorpha prisca*); their data show that the $\delta^{13}C$ values of CH_4 change with increasing temperature, depending on the type of organic matter (or CH_4 precursors). Similarly, open-system pyrolysis of immature coaly material shows that $\delta^{13}C$ of generated CH_4 becomes increasingly heavy with increasing temperature. Cramer et al. (1998) show that isotopic fractionation decreases with increasing temperature, noting that in geological systems, the strongest isotopic fractionation during gas generation would occur at low temperatures. They also suggest that, if heating continues to the point that CH_4 generation has been exhausted, then the $\delta^{13}C$ of the cumulative CH_4 depends on the initial $\delta^{13}C$ of the CH_4 precursors — in this case mostly components in vitrinite, some inertinites of semifusinitic reflectance, and very minor amounts of liptinite. The exact $\delta^{13}C$ of the precursor components is unknown, but it would be closer to that of the unaltered coal than it would be to isotopically depleted, early generated CH_4. This supports earlier work using pyrolysis that also showed that the $\delta^{13}C$ of CH_4 generated becomes heavier over time and, if taken to completion, the total accumulated CH_4 has an isotopic composition that is approximately the same as the original methane-producing components (Chung and Sackett, 1979). Additionally, heating rate influences the temperatures at which the bulk CH_4 is generated, with bulk generation occurring at higher temperatures under more rapid heating rates (Cramer et al., 1998). It is possible that under intrusive conditions, very rapid heating to very high temperatures (500–600 °C) could have instantaneously (geologically speaking!) generated all or most of the CH_4 from the coals, resulting in only minor and possibly inconsistent carbon isotopic fractionation. The very high reflectance levels of these coals, associated with multiple sills, would be consistent with this scenario.

This would suggest that, in terms of carbon isotopic fractionation, intruded coals do not behave like coals altered by normal burial maturation. Differences between coal characteristics of intruded coals verses those that have undergone normal burial maturation have been reported previously, suggesting that they follow different maturation pathways. For example, differences in VM–R_r relationships (Pearson and Murchison, 1999; Murchison, 2004, 2006; Rimmer et al., 2009; Sanders and Rimmer, 2020) (Fig. 12); H/C *versus* O/C plots (van Krevelen diagrams) (van Krevelen, 1993; Rimmer et al., 2009; Rahman and Rimmer, 2014; Presswood et al., 2016); carbon *versus* R_r relationships (Presswood et al., 2016); hydrogen *versus* carbon relationships (Presswood et al., 2016); less loss of hydrogen in intruded coals (Rahman et al., 2017); a lower degree condensation of aromatic rings in intruded coals (as determined by FTIR) (Presswood et al., 2016); density differences (Rahman et al., 2017); among others.

Additionally, in the highest reflectance samples near the sills, there is actually a slight decrease (~0.6–1‰) in $\delta^{13}C$ towards more negative values; this is especially noticeable in samples with $R_r \geq 4\%$ directly beneath the sills in cores 2 and 4. The small decreases in $\delta^{13}C$ along each profile occur in samples that contain a few percent of pyrolytic carbon. A similar decrease in $\delta^{13}C$ approaching sill contacts was reported by Cooper et al. (2007) for intruded coals in the Raton Basin, Colorado; these authors suggested that the observed accumulation of ^{12}C-rich pyrolytic carbon in the coal may be responsible. Currently, the carbon isotope composition of pyrolytic carbon is unknown, however, as this material is redeposited carbon derived from volatile gases driven off by the heat of intrusion, it is possible that pyrolytic carbon has a $\delta^{13}C$ that is slightly more negative than that of the residual coal (Meyers and Simoneit, 1999; Cooper et al., 2007). Thus, not only could there be less carbon fractionation occurring in intruded coals, but redeposition of volatiles as pyrolytic carbon may further obscure trends in $\delta^{13}C$. This raises the possibility that if alteration was very rapid and within a semi-closed system, then at least some of the volatiles had time to redeposit as pyrolytic carbon in the coal (Crelling and Dutcher, 1968; Gurba and Weber, 2001).

Controls on $\delta^{13}C$ in intruded coals appears to be fairly complex and, beyond factors that would have influenced the original coal (such as atmospheric composition, plant types, and diagenetic changes) (e.g., Gröcke, 1998, 2020; Dal Corso et al., 2011), other factors such as maceral composition, rank at the time of intrusion, extent of alteration, size of the carbon reservoir, openness of the system, and redeposition of pyrolytic carbon may have been important (see Sanders et al., 2023). Assumptions about the carbon isotopic signature of the liberated gases (e.g., CO_2, CH_4) in igneous intruded coals may not have taken these factors into consideration. A potential lack of isotopic fractionation and isotopic change in the residual coals is seen in this study and many others (e.g., Meyers and Simoneit, 1999; Cooper et al., 2007; Gröcke et al., 2009; Schimmelmann et al., 2009; Yoksoulian et al., 2016; Sanders et al., 2023). This fact should be seriously considered in studies that attempt to use igneous intrusions into coals (and/or organic-rich shales) as a mechanism to create negative carbon isotopic excursions in the geologic record (e.g., Svensen et al., 2004, 2007; McElwain et al., 2005; Retallack and Jahren, 2008).

5. Conclusions

1. Vitrinite/coke reflectance increases whereas VM and H/C decrease towards the sills. Reflectance remains higher and decreases more gradually above the sills, thus the alteration halo is significantly larger above the sills than below. The level of alteration is extensive compared to the very thin nature of the sills, especially above the sill.
2. The wide extent of the contact aureoles above the sills may suggest either prolonged magma transport within the sills and thus prolonged heat flow upwards, migration of hot fluids in fracture systems in the coals, or both.
3. Within the contact aureole a variety of coke types and carbon deposits have formed. Anisotropic coke structure (primarily fine-grained circular mosaic, with minor amounts of medium-grained circular mosaic), incipient mosaic structure, and anthracitic textures are observed in the core samples, frequently with mixed types in a single sample. The anisotropic coke structures are consistent of alteration of a high volatile A bituminous coal at the time of intrusion.
4. Vacuoles are observed close to the sills and decrease in number and size going away from the sills. Devolatilization vacuoles are better developed in altered collodetrinite than in collotelinite. Fracturing is readily seen in the coal cores; microfractures are evident under the microscope and contain minerals, coke, and pyrolytic carbon, indicating movement of fluids, fluidized coal, and volatiles throughout the altered coal.
5. In the more highly altered samples, pyrolytic carbon occurs as ribbon-like fracture fills within macerals, as linings along maceral and coke edges and within devolatilization vacuoles, as spherulites, and as botryoidal aggregates. Spherulitic forms are more abundant in the samples with very highest levels of maturation.
6 Despite the high degree of thermal alteration caused by the sills, $\delta^{13}C$ of the residual coal changes only minimally, and the overall trends in $\delta^{13}C$ are ambiguous. Possible factors affecting changes in the carbon isotopic composition of intruded coals include maceral composition, rank at the time of intrusion, extent of alteration, size of the carbon reservoir, openness of the system, and redeposition of pyrolytic carbon. It is also possible that the relatively rapid rate and extremely high temperatures of contact metamorphism could affect the amount of isotopic fractionation.

CRediT authorship contribution statement

Susan M. Rimmer: Writing – review & editing, Writing – original draft, Visualization, Supervision, Project administration, Methodology, Investigation, Formal analysis, Conceptualization. **Lois E. Yoksoulian:** Writing – review & editing, Writing – original draft, Methodology,

Investigation, Funding acquisition, Formal analysis. **Darren R. Gröcke:** Writing – review & editing, Methodology, Investigation, Formal analysis.

Declaration of competing interest

The authors declare that they have no known competing financial interests or personal relationships that could have appeared to influence the work reported in this paper.

Acknowledgments

The authors would like to thank Ry Stone and Joe Brinton of Bowie Resource Partners (Grand Junction, CO) for access to the Bowie Mine (Paonia, CO) and assistance in sampling, Chris Kravits of Kravits Geological Services for assistance in securing cores used in the study, and the Kentucky Geological Survey (Jason Backus) and the University of Kentucky Center for Applied Energy Research (CAER) for geochemical analyses. This project was partially supported by grants (to LEY) from The Society for Organic Petrology (Spackman Award), the Geological Society of America Coal (now Energy Geology) Division (Antionette Lierman Medlin Scholarship), and the Geological Society of America Southeastern Section. The authors appreciate the helpful comments from Jim Hower and two anonymous reviewers that improved the manuscript.

Data availability

Data will be made available on request.

References

ASTM (American Society for Testing and Materials), 2023. Annual Book of ASTM standards 5.06. Gaseous fuels; coal and coke. Catalysts; Bioenergy and Industrial Chemicals from Biomass 1414.
Aarnes, I., Svensen, H., Connolly, J.A.D., Podladchikov, Y.Y., 2010. How contact metamorphism can trigger global climate changes: modeling gas generation around igneous sills in sedimentary basins. Geochem. Cosmochim. Acta 74, 7179–7195.
Amijaya, H., Littke, R., 2006. Properties of thermally metamorphosed coal from Tanjung Enim Area, South Sumatra Basin, Indonesia with special reference to the coalification path of macerals. Int. J. Coal Geol. 66, 271–295.
Barker, C.E., Pawlewicz, M.J., 1994. Calculation of vitrinite reflectance from thermal histories and peak temperatures: a comparison of methods. In: Mukhopadhyay, P.K., Dow, W.G. (Eds.), Vitrinite Reflectance as a Maturity Parameter: Applications and Limitations, vol. 570. ACS Symp. Ser., pp. 216–247
Barker, C.E., Bone, Y., Lewan, M., 1998. Fluid inclusion and vitrinite-reflectance geothermometry compared to heat-flow models of maximum paleotemperature next to dikes, western onshore Gippsland Basin, Australia. Int. J. Coal Geol. 37, 73–111.
Beerling, D.J., Lomas, M.R., Gröcke, D.R., 2002. On the nature of methane gas hydrate dissociation during the Toarcian and Aptian oceanic anoxic events. Am. J. Sci. 302, 28–49.
Berner, U., Faber, E., Scheeder, G., Panten, D., 1995. Primary cracking of algal and landplant kerogens: kinetic models of isotope variations in methane, ethane and propane. Chem. Geol. 126, 233–245.
Boudou, J.-P., Pelet, R., Letolle, R., 1984. A model of the diagenetic evolution of coal sedimentary organic matter. Geochem. Cosmochim. Acta 48, 1357–1392.
Brooks, J.D., Taylor, G.H., 1968. The formation of some graphitizing carbon. In: Walker, P.L. (Ed.), Chemistry and Physics of Carbon, vol. 4. Marcel Dekker, NY, pp. 243–286.
Burgess, S.D., Muirhead, J.D., Bowring, S.A., 2017. Initial pulse of Siberian Traps sills as the trigger of the end-Permian mass extinction. Nat. Commun. 8, 164.
Carroll, C.J., 2005. Colorado coal directory 2005. Colo. Geol. Surv. Inf. Ser. 71, 68.
Carroll, C.J., Widmann, B.L., 2000. Colorado coal directory 2000. Colo. Geol. Surv. Inf. Ser. 55, 79.
Carroll, C.J., Robeck, E., Hunt, G., Koontz, W., 2004. Structural implications of the underground mining in the Mesaverde group in the Somerset coal field, Delta and Gunnison counties, Colorado. In: Nelson, E.P., Ersley, E.A. (Eds.), Field Trips in the Southern Rocky Mountains, USA, vol. 5. GSA Field Guide, pp. 41–58.
Carslaw, H.S., Jaeger, J.C., 1959. Conduction of Heat in Solids. Oxford University Press, New York, NY, p. 510.
Caruthers, A.H., Smith, P.L., Gröcke, D.R., 2013. The Pliensbachian–Toarcian (Early Jurassic) extinction, a global multi-phased event. Palaeogeogr. Palaeoclimatol. Palaeoecol. 386, 104–118.
Chandra, D., Taylor, G.H., 1982. Thermally altered coals. In: Stach, E., Mackowsky, M. Th, Teichmüller, M., Taylor, G.H., Chandra, D., Teichmüller, R. (Eds.), Coal Petrology. Gebrüder Borntrager, pp. 206–218. Berlin.
Chaudhuri, S.G., Choudhury, N., Sarkar, N.B., Bhatt, D.M., Ghose, S.P., Chatterjee, D.S., Mukherjee, D.K., 1997. The influence of pressure and hydrothermal treatment on the microtextural characteristics of coke. Carbon 35, 1457–1464.
Chung, H.M., Sackett, W.M., 1979. Use of stable carbon isotope compositions of pyrolytically derived methane as maturity indices for carbonaceous materials. Geochem. Cosmochim. Acta 43, 1979–1988.
Ciesielczuk, J., Górka, M., Fabiańska, M.J., Misz-Kennan, M., Jura, D., 2021. The influence of heating on the carbon isotope composition, organic geochemistry, and petrology of coal from the Upper Silesian Coal Basin (Poland): an experimental and field study. Int. J. Coal Geol. 241, 103749.
Cole, R., Cumella, S., 2003. Stratigraphic architecture and reservoir characteristics of the Mesaverde group, southern Piceance Basin, Colorado. Rocky Mtn. Assoc. Geologist and the AIPG Field Trip Guide Book 18, 385–442.
Conkright, M.E., Sackett, W.M., 1992. Stable carbon isotope changes during the maturation of organic matter. In: Whelan, J.K., Farrington, J.W. (Eds.), Organic Matter: Productivity, Accumulation, and Preservation in Recent and Ancient Sediments. Columbia University Press, New York, pp. 403–414.
Cooper, J.R., Crelling, J.C., Rimmer, S.M., Whittington, A.G., 2007. Coal metamorphism by igneous intrusion in the Raton Basin, CO and NM: implications for generation of volatiles. Int. J. Coal Geol. 71, 15–27.
Cramer, B., Krooss, B.M., Littke, R., 1998. Modelling isotope fractionation during primary cracking of natural gas: a reaction kinetic approach. Chem. Geol. 149, 235–250.
Crelling, J.C., 2008. Chapter 7 - coal carbonization. In: Suaréz-Ruiz, I., Crelling, J.C. (Eds.), Applied Coal Petrology. Elsevier, Burlington, pp. 173–192.
Crelling, J.C., Dutcher, R.R., 1968. A petrologic study of a thermally altered coal from the Purgatoire River Valley of Colorado. GSA Bull 79, 1375–1386.
Dal Corso, J., Preto, N., Kustatscher, E., Mietto, P., Roghi, G., Jenkyns, H.C., 2011. Carbon-isotope variability of Triassic amber, as compared with wood and leaves (Southern Alps, Italy). Palaeogeogr. Palaeoclimatol. Palaeoecol. 302, 187–193.
Dickens, G.R., Oneil, J.R., Rea, D.K., Owen, R.M., 1995. Disassociation of oceanic CH_4 hydrate as a cause of the carbon-isotope excursions at the end of the Paleocene. Paleoceanography 10, 965–971.
Falcon, R.M.S., Snyman, C.P., 1986. An introduction to coal petrography: atlas of petrographic constituents in the bituminous coals of Southern Africa. Geol. Soc. S. Africa Rev. Paper 2, 27.
Franczyk, K.J., Fouch, T.D., Johnson, R.C., Molenaar, C.M., Cobban, W.A., 1992. Cretaceous and Tertiary Paleogeographic Reconstructions for the Uinta-Piceance Basin Study Area, Colorado and Utah, 1787-Q. U.S. Geol. Surv. Bull., p. 37
Given, P.H., Yarzab, R.F., 1978. Analysis of organic substance of coals: problems posed by the presence of mineral matter. In: Karr, C. (Ed.), Analytical Methods for Coal and Coal Products, vol. II. Academic Press, New York, pp. 3–41.
Goodarzi, F., 1985a. Optical properties of vitrinite carbonized at different pressures. Fuel 64, 156–162.
Goodarzi, F., 1985b. Characteristics of pyrolytic carbon in Canadian coals. Fuel 64, 1672–1676.
Goodarzi, F., Murchison, D.G., 1978. Influence of heating-rate variation on the anisotropy of carbonized vitrinites. Fuel 57, 273–284.
Goodarzi, F., Eckstrand, O.R., Snowdon, L., Williamson, B., Stasiuk, L.D., 1992. Thermal metamorphism of bitumen in Archaen rocks by ultramafic volcanic flows. Int. J. Coal Geol. 20, 165–178.
Goodarzi, F., Gentzis, T., Jackson, G., MacQueen, R.W., 1993. Optical characteristics of heat-affected bitumens from the nanisivik mine, N.W. Baffin island, arctic Canada. Energy Sources 15, 359–376.
Goolsby, S.M., Reade, N.S., Murray, D.K., 1979. Evaluation of coking coals in Colorado. Dept. Nat. Res. Colo. Geol. Surv. Res. Ser. 7, 72.
Grasby, S.E., Sanei, H., Beauchamp, B., 2011. Catastrophic dispersion of coal fly ash into oceans during the latest Permian extinction. Nat. Geosci. 4, 104–107.
Gröcke, D.R., 1998. Carbon-isotope analyses of fossil plants as a chemostratigraphic and palaeoenvironmental tool. Lethaia 31, 1–13.
Gröcke, D.R., 2020. Carbon isotope stratigraphy – principles and applications. Stratigr. Timesc. 5, 1–40.
Gröcke, D.R., Rimmer, S.M., Yoksoulian, L.E., Cairncross, B., Tsikos, H., 2009. No evidence for large-scale thermogenic methane release by the Karoo-Ferrar large igneous province. Earth Planet Sci. Lett. 277, 204–212.
Gurba, L.W., Weber, C.R., 2001. Effects of igneous intrusions on coalbed methane potential, Gunnedah Basin, Australia. Int. J. Coal Geol. 46, 113–131.
Hesselbo, S.P., Gröcke, D.R., Bjerrum, C.J., Farrimond, P., Morgans-Bell, H.S., Green, O. G., 2000. Massive dissociation of gas hydrate during a Jurassic oceanic anoxic event. Nature 406, 392–395.
Hettinger, R.D., Roberts, L.N.R., Gognat, T.A., 2000. Investigations of the distribution and resources of coal in the southern part of the Piceance Basin, Colorado. In: Chapter, O., Kirschbaum, M.A., Roberts, L.N.R., Biewick, L.R.H. (Eds.), Geologic Assessment of Coal in the Colorado Plateau: Arizona, Colorado, New Mexico, and Utah: U.S.G.S. Prof. Paper 1625–B.
Higgins, J.A., Schrag, D.P., 2006. Beyond methane: towards a theory for the paleocene-eocene thermal maximum. Earth Planet Sci. Lett. 245, 523–537.
Hoefs, J., Frey, M., 1976. The isotopic composition of carbonaceous matter in a metamorphic profile from the Swiss Alps. Geochem. Cosmochim. Acta 40, 945–951.
Hower, J.C., Rimmer, S.M., Mastalerz, M., Wagner, N.J., 2019. Notes on the mechanisms of coal metamorphism in the Pennsylvania Anthracite Fields. Int. J. Coal Geol. 202, 161–170.
Hower, J.C., Rimmer, S.M., Mastalerz, M., Wagner, N.J., 2021. Migmatite-like textures in anthracite: further evidence for low-grade metamorphic melting and resolidification in high-rank coals. Geosci. Front. 12, 101122.

Hunt, J.M., 1996. Petroleum Geochemistry and Geology, second ed. W.H. Freeman and Company, New York, NY, p. 743.
Johnson, R.C., Nuccio, V.F., 1986. Structural and thermal maturity of the Piceance Creek basin, western Colorado, in relationship to hydrocarbon occurrence in the Mesaverde Group. In: Spencer, C.W., Mast, R.F. (Eds.), Geology of Tight Gas Reservoirs: AAPG Stud. Geol., vol. 24, pp. 165–206.
Jüntgen, H., Karweil, J., 1966. Gasbildung und Gasspeicherung in Steinkohlenflozen. I: Gasbildung. Erdol Kohle 19, 251–258.
Kisch, H.J., Taylor, G.H., 1966. Metamorphism and alteration near an intrusive-coal contact. Econ. Geol. 61, 343–361.
Krull, E.S., Retallack, G.J., Campbell, H.J., Lyon, G.L., 2000. $\delta^{13}C_{org}$ chemostratigraphy of the Permian-Triassic boundary in the Maitai Group, New Zealand: evidence for high-latitudinal methane release. N. Z. J. Geol. Geophys. 43, 21–32.
Krull, E.S., Lehrmann, D.J., Druke, D., Kessel, B., Yu, Y.-Y., Li, R.-X., 2004. Stable carbon isotope stratigraphy across the Permian-Triassic boundary in shallow marine platforms, Nanpanjiang Basin, south China: palaeogeogr. Palaeoclimat. Palaeoecol. 204, 297–315.
Kwiecińska, B.K., Petersen, H.I., 2004. Graphite, semi-graphite, natural coke, and natural char classification – ICCP system. Int. J. Coal Geol. 57, 99–116.
Kwiecińska, B.K., Pusz, S., 2016. Pyrolytic carbon – definition, classification and occurrence. Int. J. Coal Geol. 163, 1–7.
Knopf, A., 1926. Recent Developments in the Aspen District, Colorado, 785–A. U.S.G.S. Bull., pp. 1–28
Li, K., Rimmer, S.M., Liu, Q., 2018. Geochemical and petrographic analysis of graphitized coals from Central Hunan, China. Int. J. Coal Geol. 195, 267–279.
Mastalerz, M., Schimmelmann, A., 2002. Isotopically exchangeable organic hydrogen in coal relates to thermal maturity and maceral composition. Org. Geochem. 33, 921–931.
McElwain, J.C., Wade-Murphy, J., Hesselbo, S.P., 2005. Changes in carbon dioxide during an oceanic anoxic event linked to intrusion into Gondwana coals. Nature 435, 479–482.
McInerney, F.A., Wing, S.L., 2011. The Paleocene–Eocene Thermal Maximum: a perturbation of carbon cycle, climate, and biosphere with implications for the future. Annu. Rev. Earth Planet Sci. 39, 489–516.
McKirdy, D.M., Powell, T.G., 1974. Metamorphic alteration of carbon isotopic composition in ancient sedimentary organic matter. New evidence from Australia and South Africa. Geology 2, 591–595.
Meyers, P.A., Simoneit, B.R.T., 1999. Effects of extreme heating on the elemental and isotopic compositions of an Upper Cretaceous coal. Org. Geochem. 30, 299–305.
Moroeng, O.M., 2022. Effects of contact metamorphism on $\delta^{13}C$, $\delta^{15}N$, and XPS nitrogen functional forms of inertinite-rich Witbank coals (South Africa): indications for possible alteration by hydrothermal fluids. Chem. Geol. 612, 121135.
Murchison, D., 2004. Aberrations in the coalification patterns of the offshore coalfields of Northumberland and Durham, United Kingdom. Int. J. Coal Geol. 58, 133–146.
Murchison, D., 2006. The influence of heating rates on organic matter in laboratory and natural environments. Int. J. Coal Geol. 67, 145–157.
Obradovich, J.D., Mutschler, F.E., Bryant, B., 1969. Potassium-argon ages bearing on the igneous and tectonic history of the Elk Mountains and vicinity, Colorado: a preliminary report. GSA Bull 80, 1749–1756.
Pagani, M., Caldeira, K., Archer, D., Zachos, J.C., 2006. An ancient carbon mystery. Science 314, 1556–1557.
Pearson, D., Murchison, D., 1999. Relationship between reflectance and volatile-matter yield at the Maudlin (H) horizon of the offshore Northumberland and Durham coalfields. Fuel 78, 1417–1423.
Podwysocki, M.H., Dutcher, R.R., 1971. Coal dikes that intrude lamprophyre sills; Purgatoire River Valley, Colorado. Econ. Geol. 66, 267–280.
Pontolillo, J., Stanton, R.W., 1994. Coal petrographic laboratory procedures and safety manual, II. U.S.G.S. Open-File Rept. Inv. 94–631.
Presswood, S.M., Rimmer, S.M., Anderson, K.B., Filiberto, J., 2016. Geochemical and petrographic alteration of rapidly heated coals from the Herrin (No. 6) coal seam, Illinois Basin. Int. J. Coal Geol. 165, 243–256.
Rahman, M.W., Rimmer, S.M., 2014. Effects of rapid thermal alteration on coal: geochemical and petrographic signatures in the Springfield (No. 5) Coal, Illinois Basin. Int. J. Coal Geol. 131, 214–226.
Rahman, M.W., Rimmer, S.M., Rowe, H.D., Huggett, W.W., 2017. Carbon isotope analysis of whole-coal and vitrinite from intruded coals from the Illinois Basin: no isotopic evidence for thermogenic methane generation. Chem. Geol. 453, 1–11.
Rahman, M.W., Rimmer, S.M., Rowe, H.D., 2018. The impact of rapid heating by intrusion on the geochemistry and petrography of coals and organic-rich shales in the Illinois Basin. Int. J. Coal Geol. 187, 45–53.
Rampino, M.R., Rodriguez, S., Baransky, E., Cai, Y., 2017. Global nickel anomaly links Siberian Traps eruptions and the latest Permian mass extinction. Sci. Rep. 7, 12416.
Retallack, G.J., Jahren, A.H., 2008. Methane release from igneous intrusion of coal during late permian extinction events. J. Geol. 116, 1–20.
Rimmer, S.M., Rowe, H.D., Taulbee, D.N., Hower, J.C., 2006. Influence of maceral content on $\delta^{13}C$ and $\delta^{15}N$ in a Middle Pennsylvanian coal. Chem. Geol. 225, 77–90.
Rimmer, S.M., Yoksoulian, L.E., Hower, J.C., 2009. Anatomy of an intruded coal, I: effect of contact metamorphism on whole-coal geochemistry, Springfield (No. 5) (Pennsylvanian) coal, Illinois Basin. Int. J. Coal Geol. 79, 74–82.
Rimmer, S.M., Crelling, J.C., Yoksoulian, L.E., 2015. An occurrence of coked bitumen, Raton formation, purgatoire river valley, Colorado, USA. Int. J. Coal Geol. 141–142, 63–73.
Robeck, E.D., 2005. The Effects of Fault-Induced Stress Anisotropy on Fracturing, Folding and Sill Emplacement: Insights from the Bowie Coal Mines, Southern Piceance Basin, Western Colorado. Unpubl. M.S. Thesis, Brigham Young Univ., Provo, UT, p. 94.
Roberts, L.N.R., Kirschbaum, M.A., 1995. Paleogeography of the late cretaceous of the western interior of middle north America—coal distribution and sediment accumulation. U.S.G.S. Prof. Pap. 1561, 115.
Sackett, W.M., 1978. Carbon and hydrogen isotope effects during the thermocatalytic production of hydrocarbons in laboratory simulation experiments. Geochem. Cosmochim. Acta 42, 571–580.
Sanborn, A.F., 1977. Possible future petroleum of Unita and Piceance basins and vicinity northeast Utah and northwest Colorado. AAPG Spec. Vol. M 15: Future Petroleum Provinces of the United States - Their Geology and Potential 1, 489–508.
Sanders, M.M., Rimmer, S.M., 2020. Revisiting the thermally metamorphosed coals of the Transantarctic Mountains, Antarctica. Int. J. Coal Geol. 228, 103550.
Sanders, M.M., Rimmer, S.M., Rowe, H.D., 2023. Carbon isotopic composition and organic petrography of thermally metamorphosed Antarctic coal: implications for evaluation of $\delta^{13}C_{org}$ excursions in paleo-atmospheric reconstruction. Int. J. Coal Geol. 267, 104182.
Saxby, J.D., Stephenson, L.C., 1987. Effect of an igneous intrusion on oil shale at Rundle (Australia). Chem. Geol. 63, 1–16.
Schapiro, N., Gray, R.J., 1966. Physical variations in highly metamorphosed Antarctic coals. In: Gould, R.F. (Ed.), Adv. Chem. 55, 196–210. Coal Science, Amer. Chem. Soc.
Schimmelmann, A., Mastalerz, M., Ling, G., Sauer, P., Topalov, K., 2009. Dike intrusions into bituminous coal: H, C, N, O isotopic responses to rapid and brief heating. Geochem. Cosmochim. Acta 73, 6264–6281.
Singh, A.K., Singh, M.P., Sharma, M., Srinivastava, S.K., 2007. Microstructures and microtextures of natural cokes: a case study of the heated-affected coking coals from the Jharia coalfield, India. Int. J. Coal Geol. 71, 153–175.
Singh, A.K., Sharma, M., Singh, M.P., 2013. SEM and reflected light petrography: a case study on natural cokes from seam XIV, Jharia coalfield, India. Fuel 112, 502–512.
Svensen, H., Pank, S., Malthe-Sørenssen, A., Jamtveit, B., Myklebust, R., Rassmussen Eidem, T., Rey, S.S., 2004. Release of CH_4 from a volcanic basin as a mechanism for the initial Eocene global warming. Nature 429, 542–545.
Svensen, H., Planke, S., Chevallier, L., Malthe-Sørenssen, A., Corfu, F., Jamtveit, B., 2007. Hydrothermal venting of greenhouse gases triggering Early Jurassic global warming. Earth Planet Sci. Lett. 256, 554–566.
Taylor, G.H., Teichmüller, M., Davis, A., Diessel, C.F.K., Littke, R., Robert, P., 1998. Organic Petrology. Gebrüder Borntraeger, Berlin, p. 704.
Taylor, G.H., 1961. Development of optical properties of coke during carbonization. Fuel 40, 465–472.
Trabucho-Alexandre, J.P., Gröcke, D.R., Atar, E., Herringshaw, L., Jarvis, I., 2022. A new subsurface record of the pliensbachian-toarcian, lower Jurassic, of Yorkshire. In: Proc. Yorkshire Geol. Soc., vol. 64. pygs 2022, p. 7.
van Krevelen, D.W., 1993. Coal: typology, chemistry. Physics, Constitution, third ed. Elsevier, Amsterdam, p. 979.
Wang, D., Lu, X., Xu, S., Hu, W., 2008. Comment on "Influence of basic intrusion on the vitrinite reflectance and chemistry of the Springfield (No. 5) coal, Harrisburg, Illinois" by Stewart et al. (2005). Int. J. Coal Geol. 73, 196–199.
Wang, L., Cao, D., Peng, Y., Ding, Z., Li, Y., 2019. Stain-induced graphitization mechanism of coal-based graphite form Lutang, Hunan Province, China. Minerals 9, 617.
Wang, N., Esterle, J.S., Rodrigues, S., Hower, J.C., Dai, S., 2024. Insights on the regional thermal evolution from semianthracite petrology of the Fengfeng coalfield, China. Int. J. Coal Geol. 290, 104548.
Whiticar, M.J., 1996. Stable isotope geochemistry of coals, humic kerogens and related natural gases. Int. J. Coal Geol. 32, 191–215.
Yoksoulian, L.E., 2010. Effect of Contact Metamorphism on Coal Geochemistry and Petrology: Implications for the Large-Scale Release of ^{12}C–Enriched Methane. Unpubl. Ph.D. Dissertation, Univ. Kentucky, Lexington, KY, p. 133.
Yoksoulian, L.E., Rimmer, S.M., Rowe, H.D., 2016. Anatomy of an intruded coal, II: effect of contact metamorphism on organic $\delta^{13}C$ and implications for the release of thermogenic methane, Springfield (No. 5) coal, Illinois Basin. Int. J. Coal Geol. 158, 129–136.